

UC Irvine

UC Irvine Previously Published Works

Title

PP4-dependent HDAC3 dephosphorylation discriminates between axonal regeneration and regenerative failure

Permalink

<https://escholarship.org/uc/item/3bg4t08q>

Journal

The EMBO Journal, 38(13)

ISSN

0261-4189

Authors

Hervera, Arnau
Zhou, Luming
Palmisano, Ilaria
et al.

Publication Date



2019-07-01

DOI

10.15252/emj.2018101032

Peer reviewed

PP4-dependent HDAC3 dephosphorylation discriminates between axonal regeneration and regenerative failure

Arnau Hervera^{1,2,3,4,5,†}, Luming Zhou^{1,6,7,†}, Ilaria Palmisano¹, Eilidh McLachlan¹, Guiping Kong^{1,6}, Thomas H Hutson¹, Matt C Danzi⁸, Vance P Lemmon⁸ , John L Bixby⁸, Andreu Matamoros-Angles^{2,3,4,5}, Kirsi Forsberg⁶, Francesco De Virgiliis^{1,6,7}, Dina P Matheos⁹, Janine Kwapis⁹, Marcelo A Wood⁹, Radhika Puttagunta^{6,10}, José Antonio del Río^{2,3,4,5} & Simone Di Giovanni^{1,6,*} 

Abstract

The molecular mechanisms discriminating between regenerative failure and success remain elusive. While a regeneration-competent peripheral nerve injury mounts a regenerative gene expression response in bipolar dorsal root ganglia (DRG) sensory neurons, a regeneration-incompetent central spinal cord injury does not. This dichotomic response offers a unique opportunity to investigate the fundamental biological mechanisms underpinning regenerative ability. Following a pharmacological screen with small-molecule inhibitors targeting key epigenetic enzymes in DRG neurons, we identified HDAC3 signalling as a novel candidate brake to axonal regenerative growth. *In vivo*, we determined that only a regenerative peripheral but not a central spinal injury induces an increase in calcium, which activates protein phosphatase 4 that in turn dephosphorylates HDAC3, thus impairing its activity and enhancing histone acetylation. Bioinformatics analysis of *ex vivo* H3K9ac ChIPseq and RNAseq from DRG followed by promoter acetylation and protein expression studies implicated HDAC3 in the regulation of multiple regenerative pathways. Finally, genetic or pharmacological HDAC3 inhibition overcame regenerative failure of sensory axons following spinal cord injury. Together, these data indicate that PP4-dependent HDAC3 dephosphorylation discriminates between axonal regeneration and regenerative failure.

Keywords calcium; HDAC3; nerve regeneration; spinal cord injury; transcription

Subject Categories Neuroscience; Signal Transduction

DOI 10.15252/embj.2018101032 | Received 29 October 2018 | Revised 15 April 2019 | Accepted 17 April 2019 | Published online 22 May 2019

The EMBO Journal (2019) 38: e101032

Introduction

Following a central nervous system (CNS) injury, such as stroke or spinal cord injury, axonal regeneration is highly restricted. In stark contrast, spontaneous albeit partial functional axonal regeneration is possible after a peripheral nervous system (PNS) injury. This is likely due to the differences of the CNS and PNS in both intrinsic properties of neurons and the surrounding cellular environment. Importantly, glial cell-dependent signalling can affect the intrinsic properties of neurons (Puttagunta *et al*, 2011), as is evident by the fact that the neuronal regenerative gene expression programme is only activated when axons lie within the PNS, but not in the CNS. This is typically modelled by the lumbar dorsal root ganglion (DRG) neurons (Neumann & Woolf, 1999; Teng & Tang, 2006), which project a peripheral axonal branch into the sciatic nerve (consisting of a permissive cellular environment) and a central axonal branch into the spinal cord (consisting of an inhibitory cellular environment). Strikingly, the peripheral branch of DRG mounts a robust regenerative response following a sciatic nerve injury, while the central branch fails to regenerate following a spinal injury (Neumann & Woolf, 1999; Neumann *et al*, 2002). Furthermore, regeneration of the CNS branch is greatly enhanced by prior injury to the

1 Department of Medicine, Division of Brain Sciences, Molecular Neuroregeneration, Imperial College London, London, UK

2 Molecular and Cellular Neurobiotechnology, Institute for Bioengineering of Catalonia (IBEC), Parc Científic de Barcelona, Barcelona, Spain

3 Centro de Investigación Biomédica en Red sobre Enfermedades Neurodegenerativas (CIBERNED), Barcelona, Spain

4 Department of Cell Biology, Physiology and Immunology, Universitat de Barcelona, Barcelona, Spain

5 Institute of Neuroscience, University of Barcelona, Barcelona, Spain

6 Laboratory for NeuroRegeneration and Repair, Center for Neurology, Hertie Institute for Clinical Brain Research, University of Tuebingen, Tuebingen, Germany

7 Graduate School for Cellular and Molecular Neuroscience, University of Tuebingen, Tuebingen, Germany

8 The Miami Project to Cure Paralysis, Department of Neurological Surgery, Miller School of Medicine, University of Miami, Miami, FL, USA

9 Center for the Neurobiology of Learning & Memory, Department of Neurobiology & Behavior, University of California, Irvine, CA, USA

10 Spinal Cord Injury Center, University Hospital Heidelberg, Heidelberg, Germany

*Corresponding author. Tel: +44 020 759 43178; E-mail: s.di-giovanni@imperial.ac.uk

†These authors contributed equally to this work

peripheral branch (conditioning lesion; Neumann & Woolf, 1999; Neumann *et al*, 2002) that leads to an increase in gene expression of a number of axonal growth and regeneration-associated genes, which does not occur after spinal lesions alone (Chong *et al*, 1994; Tonra *et al*, 1998; Zhang *et al*, 2000; Mason *et al*, 2002; McGraw *et al*, 2004; Stam *et al*, 2007).

Dynamic gene expression changes are controlled and coordinated by epigenetic regulation such as DNA methylation or histone post-translational modifications which are essential in stem cell reprogramming, development of tissues and organs, as well as cancer initiation (Kretsovali *et al*, 2012). Strategies that take advantage of broad histone deacetylase (HDAC) inhibitory drugs (classes I and II such as TSA or MS-275) have been poor in promoting axonal regeneration after an optic nerve crush (Gaub *et al*, 2011) or in enhancing regeneration past the lesion site after a spinal cord injury (Finelli *et al*, 2013). Recently, we found that ERK-dependent phosphorylation leads to acetylation of histone H3K9 at the promoters of select RAGs after sciatic injury (Puttagunta *et al*, 2014) and that viral overexpression of P300/CBP-associated factor (P/CAF) promotes axonal regeneration after spinal cord injury by reactivating a regenerative gene expression programme (Puttagunta *et al*, 2014). We also recently investigated DNA methylation in DRG following sciatic nerve versus spinal injury by methylation arrays including the CpG island-rich promoter region of 13,000 genes and found that DNA methylation was not differentially represented on regeneration-associated genes (Lindner *et al*, 2014). However, this study fell short of providing genomewide DNA methylation profiles; therefore, it did not allow ruling out a role for DNA methylation in axonal regeneration.

However, whether specific axonal signalling mechanisms can discriminate between axonal regeneration and regenerative failure by differentially activating or restricting the regenerative programme remains elusive. Here, we hypothesize that critical axonal signals are conveyed to modify gene expression to restrict the regeneration programme after a non-regenerative spinal lesion, while these restrictions are lifted following a regenerative peripheral injury. Since regulation of gene expression relies on enzymes whose function is controlled by their activity, initially we adopted a pharmacological small-molecule inhibitor screen of key epigenetic enzymes aiming to identify signalling pathways that might influence the regenerative growth potential of primary adult neurons and overcome regenerative failure. From this screen, we discovered that HDAC3 inhibition promoted neurite outgrowth on both growth-permissive and inhibitory substrates. Next, we found that a regeneration-competent sciatic nerve injury induces an increase in calcium that activates protein phosphatase 4 (PP4) and slightly increases the activity of protein phosphatase 2 (PP2), which in turn dephosphorylates HDAC3, inhibiting its activity. However, a spinal lesion does not elicit increases in calcium signalling nor PP activity therefore failing to dephosphorylate HDAC3. Inhibition of PP4/2 activity promotes DRG regenerative growth similarly to mimicking HDAC3 phosphorylation.

Combined bioinformatics analysis of H3K9ac ChIPseq and RNAseq from DRG as well as HDAC3 protein-protein interaction databases suggested that HDAC3 might restrict the regenerative programme. Indeed, we found that inhibition of HDAC3 activity engages several regeneration-associated signalling pathways. Finally, we translated these findings to *in vivo* models of spinal cord

injury where we found that either AAV-mediated overexpression of HDAC3 deacetylase-dead mutant or pharmacological HDAC3 inhibition overcomes regenerative failure by promoting axonal growth of sensory axons. In summary, we found that calcium activation of PP4 leading to HDAC3 dephosphorylation discriminates between axonal regeneration and regenerative failure.

Results

Pharmacological inhibition and genetic manipulation show that HDAC3 inhibition selectively enhances neurite outgrowth on both growth-permissive and non-permissive substrates

We performed a compound screen to identify whether inhibiting the activities of enzymes that modify key epigenetic marks could promote neurite outgrowth of adult neurons on both growth-permissive and non-permissive inhibitory substrates. All inhibitors were initially screened at various concentrations in a neurite outgrowth assay using adult mouse dorsal root ganglia (DRG) neurons cultured on a growth-permissive laminin-PDL substrate. The inhibitors that promoted significant outgrowth were further examined on a myelin growth inhibitory substrate.

We screened 14 pharmacological inhibitors of enzymes affecting epigenetic marks (Table 1, Fig EV1A). These include inhibitors of DNMT1-3, DNMT3b, HDAC class II (HDAC4, 5, 7, 9), HDAC1, HDAC1-2, HDAC3, the HMT G9a for H3K9me3, EZH2 for H3K27me3, DOT1L for H3K79me3, the HKDM JMJD2 for H3K9me3, JMJD3 for H3K27me3 and the HDR PADI4 for H3R2-8-17cit. Inhibitors of bromodomain BRD2/3/4 and BAZ2 proteins that are linked to both permissive and repressive epigenetic marks were also examined. The EZH2 inhibitor 503 and the HDAC3 inhibitor *RGFP966* significantly enhanced neurite outgrowth by more than twofold compared to vehicle. However, only *RGFP966*-dependent HDAC3 inhibition resulted in significant and extensive neurite outgrowth

Table 1. List of inhibitory drugs, target molecule and epigenetic mark employed in a screening for DRG neurite outgrowth.

Drug	Enzyme	Target	Function
5-AZA	DNMT1/3	DNMT	5'-Methylcytosine
13X	DNMT3B	DNMT	5'-Methylcytosine
69A	HDAC class II (4/5/7/9)	HDAC	H3/4ac
233	HDAC1	HDAC	H3/4ac
963	HDAC1/2	HDAC	H3/4ac
966	HDAC3	HDAC	H3/4ac
801	BAZ2A/BAZ2B	HME/DNMT	H3/4ac
51A	BRD 2/3/4	S/T kin	H3K79me3
17A	DOT1L	HMT	H3K27me3
J4/77A	JMJD3	HKDM	H3K9me3
71B	G9A	HMT	H3R(2/8/17)cit
484	PADI4	HDI/HRMD	H3K9me3/36me3/4me3
67A	JMJD2/JARID1	HKDM	H3K9me3
503	EZH2	HMT	H3K27me3

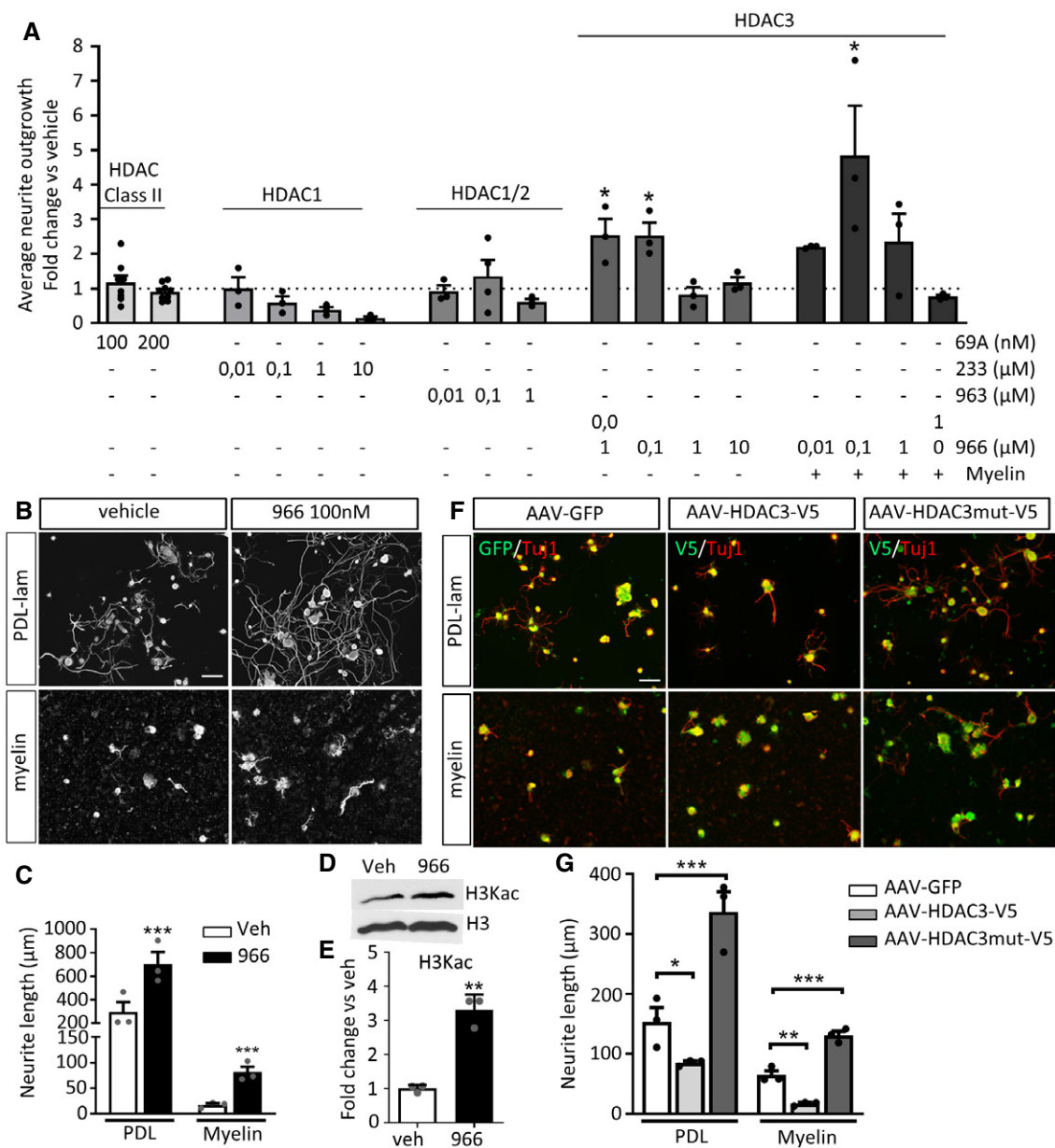


Figure 1. Pharmacological HDAC3 inhibition and HDAC3 dead mutant enhance DRG neurite outgrowth.

A RGFP966 (966)-dependent HDAC3 inhibition resulted in significant and robust neurite outgrowth (24 h in culture) compared to HDAC class II, HDAC1/2 and HDAC1 or 3 inhibitions via 69A, 963 and 233, respectively.

B, C Specific pharmacological inhibition of HDAC3 facilitates DRG neurite outgrowth (average neurite outgrowth after 24 h in culture, Tuj1-positive neurons) on PDL-laminin or myelin substrates. Scale bars, 100 μm.

D, E Immunoblotting shows significantly increased H3K9 acetylation after 966 vs. vehicle.

F, G AAV-mediated mutant HDAC3 (Y298H, V5) infection of DRG neurons induces neurite outgrowth (Tuj1/V5 double-positive neurons) after 36 h in culture, which is repressed by wild-type HDAC3 overexpression. Scale bars, 100 μm.

Data information: Data are expressed as mean fold change or average neurite length ± s.e.m. *N* = 3–9 biological replicates. **P* < 0.05, ***P* < 0.01, ****P* < 0.005 indicate significant difference of 966 versus vehicle or V5 vs. AAV-GFP (C and E, Student's *t*-test) (A and G, ANOVA followed by Bonferroni test).

Source data are available online for this figure.

on both permissive laminin and inhibitory myelin substrates (Fig 1A–C), and enhanced H3K9 acetylation as expected (Fig 1D and E). In contrast, inhibitors of HDAC class II or HDAC1 (233) and HDAC1-2 (963) did not affect DRG outgrowth, although they increased overall histone acetylation as expected (Figs 1A and EV1B

and C). Next, we infected cultured DRG neurons plated on PDL-laminin or myelin with an AAV-HDAC3 deacetylase-dead mutant (HDAC3mut), a control AAV-GFP or AAV-HDAC3wt. We found that while overexpression of wt HDAC3 restricted outgrowth, overexpression of mutant HDAC3 strongly promoted neurite outgrowth on both

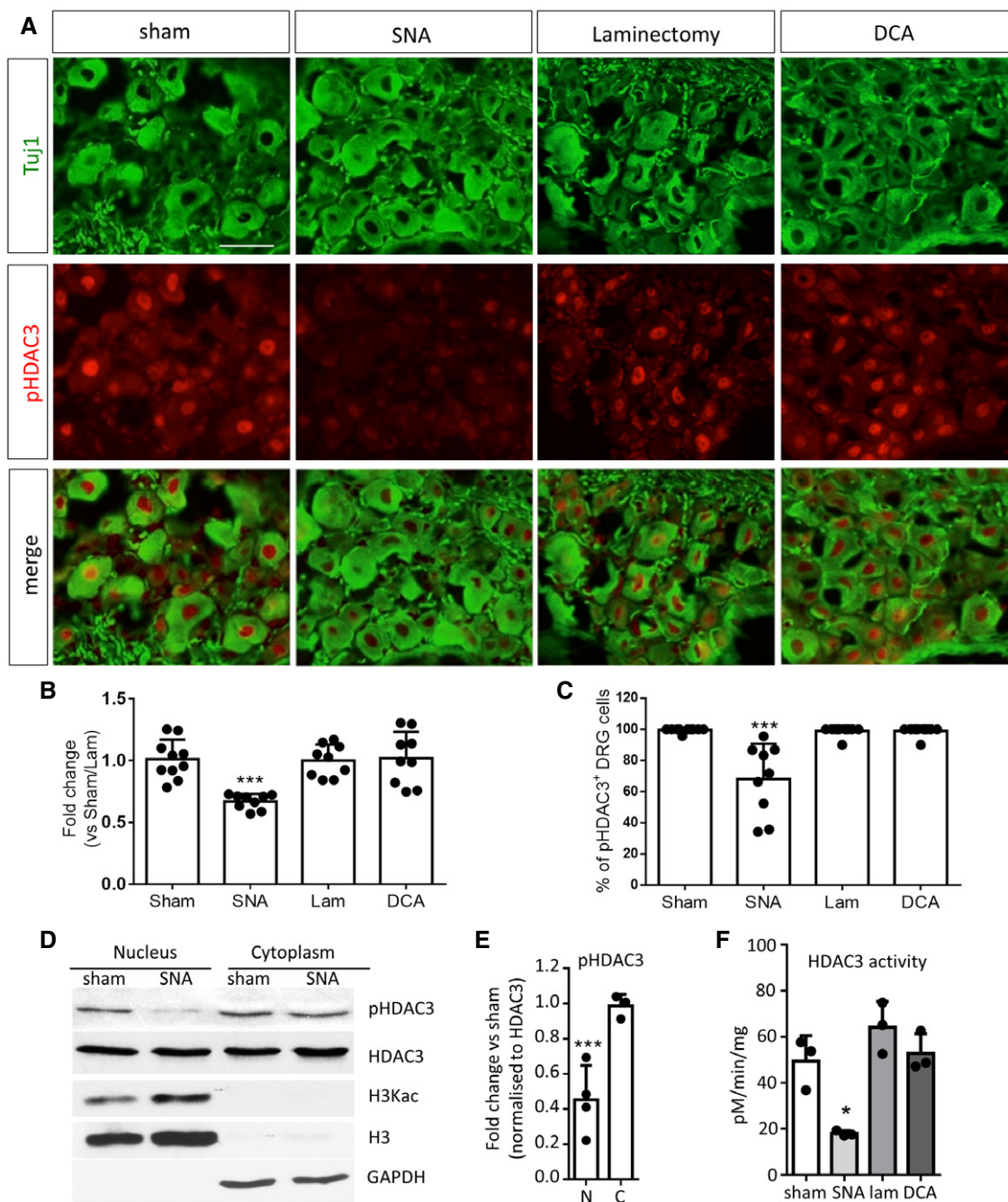


Figure 2. Regenerative sciatic nerve injury selectively decreases HDAC3 phosphorylation and activity in DRG neurons.

A IHC in DRG sections for pHDAC3 revealed that HDAC3 phosphorylation is decreased, primarily in the nucleus 24 h after sciatic nerve axotomy (SNA) but not spinal dorsal column axotomy (DCA). Scale bars, 100 μ m.

B, C Bar graphs show mean fold change levels (**B**) or % of pHDAC3⁺ cells (**C**) (pHDAC3⁺ threshold was set at the minimum intensity level of sham cells) \pm s.e.m. DAPI counterstaining was used to label nuclei $N = 9-10$ biological replicates. *** $P < 0.005$ indicate significant difference versus sham or laminectomy (lam) (ANOVA followed by Bonferroni test).

D Western blot revealed that HDAC3 phosphorylation is decreased in DRG nuclear extracts but not in the cytoplasm 24 h after SNA.

E Bar graphs show intensity measurement of nuclear vs. cytoplasm immunoblot. Data are expressed as mean \pm s.e.m. $N = 3$ biological replicates. *** $P < 0.005$ indicate significant difference versus sham (Student's *t*-test).

F HDAC3 activity (HDAC3 IP and activity assay) is strongly reduced after SNA but not DCA. Data are expressed as mean \pm s.e.m. $N = 3$ biological replicates. * $P < 0.05$ indicate significant difference versus sham (ANOVA followed by Bonferroni test).

Source data are available online for this figure.

permissive and inhibitory substrates and enhanced histone acetylation (Figs 1F and G, and EV1D and E). Similarly, HDAC3 gene silencing with validated shRNAs promoted DRG outgrowth (Fig EV1F and G), supporting the HDAC3 pharmacological inhibition and deacetylase mutant overexpression data. This indicates that HDAC3 may be a repressor of axonal regeneration whose inhibition might allow gene expression-dependent regenerative reprogramming.

HDAC3 phosphorylation and activity are inhibited by a peripheral sciatic but not by a central spinal injury

Next, we investigated the post-injury regulation of HDAC3 in the pseudo-unipolar DRG system *in vivo* following a regeneration-competent peripheral sciatic nerve axotomy (SNA) injury versus a regeneration-incompetent central spinal axotomy (DCA). This allowed for the comparison of HDAC3 regulation in the same neuronal population undergoing a regenerative versus non-regenerative axonal lesion. HDAC3 can be regulated at the gene or protein expression level; it can be shuttled between cytoplasm and nucleus; and it can be phosphorylated (Zhang *et al*, 2005; Karagianni & Wong, 2007; Togi *et al*, 2009). First, we measured the gene expression of HDAC3 and of the other class I HDACs, HDAC1 and HDAC2 by qPCR, in sham versus axonal injury in DRG. We found that all HDACs are expressed in DRGs, but neither a peripheral nor a central injury modifies their gene expression level (Appendix Fig S1A and B). Protein analysis of HDAC3 expression revealed that it is highly expressed in DRG neurons, mainly in the nucleus, but again neither its protein expression nor its nuclear–cytoplasmic shuttling was regulated by either a sciatic or a spinal injury (Fig EV2A–E). However, we found that the nuclear phosphorylation of HDAC3 (Ser424) was strongly reduced by a sciatic but not by a central spinal injury (Fig 2A–E). Since phosphorylation of HDAC3 promotes its enzymatic activity, we measured the activity of HDAC3 in DRG after DCA or SNA to find that HDAC3 deacetylase activity was strongly reduced by SNA only (Fig 2F), in line with its reduced phosphorylation.

Sciatic nerve but not spinal injury induces calcium-dependent PP4 activity that is required for HDAC3 dephosphorylation

Calcium is a prominent second messenger triggered by the regenerative sciatic nerve injury, although whether it fails to be induced in DRG by a central spinal injury remains elusive. Protein phosphatases 4c and 2a (PP4c and PP2a) are activated via calcium signalling and have been shown to interact with HDAC3. However, only PP4c has been shown to dephosphorylate HDAC3 in cancer cells (Zhang *et al*, 2005; Togi *et al*, 2009); nonetheless, whether PP4c and PP2a control HDAC3 phosphorylation in neurons has not been investigated. Therefore, we hypothesized that a regenerative peripheral SNA but not a central DCA would lead to calcium-dependent activation of PP4c and/or PP2a. This would in turn inhibit HDAC3 via dephosphorylation resulting in an increase in histone acetylation in DRG neurons. First, we measured the activity of PP4c or PP2a following SNA or DCA. We found that SNA but not DCA strongly promoted calcium-dependent PP4c and PP2a activity that was inhibited by administration of the calcium chelator EGTA (Fig 3A and B). Accordingly, we also found that calcium, required for PP activity, was induced by SNA but remained unchanged following DCA (Fig 3C). While PP4c basal activity was very low in

DRG and was strongly induced by SNA (Fig 3A), PP2a basal levels were higher (Fig 3B), suggesting that PP4c is the preferentially inducible protein phosphatase selectively following SNA. Moreover, the calcium chelator EGTA was able to block the injury-induced increase in PP4c and PP2a activity, highlighting the calcium dependence of the phosphatase activity induced by SNA. We next investigated whether phosphorylation of HDAC3 in DRG was also dependent upon calcium. Indeed, we found that HDAC3 dephosphorylation after sciatic nerve injury required calcium, as administration of EGTA on the nerve at the time of injury blocked nuclear HDAC3 dephosphorylation without altering HDAC3 expression (Fig 3D–F). In support of these findings, we observed a significant correlation between HDAC3 dephosphorylation but not total HDAC3 and calcium signal intensity after potassium chloride (KCl)-dependent calcium induction in DRG neurons (Fig EV3A–E). Additionally, when we inhibited PP4/2a activity with the PP4/2a inhibitor Fostriecin in KCl-treated DRG cells, we observed that the correlation between calcium and HDAC3 dephosphorylation or histone acetylation was lost (Fig 3G and H). Next, we asked whether PP4/2a activity was required for HDAC3 dephosphorylation and for DRG regenerative growth. We delivered PP4/2a inhibitor Fostriecin or vehicle intrathecally immediately after sham or SNA; 24 hours later, we measured HDAC3 phosphorylation and H3K9ac in DRG or performed a neurite outgrowth assay in cultured DRG neurons. Importantly, first we found that PP4/2a inhibition led to an increase in HDAC3 phosphorylation with a concomitant decrease in H3K9ac in DRG neurons (Fig 3I–L). Next, we observed that PP4/2a inhibition blocked SNA-dependent DRG regenerative growth (Fig 3M and N). When we silenced PP4c or PP2a by nucleofection of siRNA against PP4c or PP2a in KCl-treated DRG cells, we observed that KCl-dependent HDAC3 dephosphorylation was significantly reduced (Fig 4A–G). Antibodies to PP2a were available for Western blotting and antibodies to PP4 were available for immunocytochemistry (ICC) only, determining the choice of the protein detection system including after silencing. We finally asked whether HDAC3 serine 424 phosphorylation (ser424) that controls HDAC3 activity and histone acetylation (Kwapis *et al*, 2017) is able to regulate DRG outgrowth. We overexpressed phospho-mimetic or phospho-dead HDAC3 S424A or S424D mutant plasmids in cultured DRG cells, respectively. As expected, while HDAC3 phospho-dead S424A significantly promoted DRG outgrowth compared to control vector or HDAC3 WT, phospho-mimetic HDAC3 S424D inhibited it (Fig 4H and I). All together, these data suggest that peripheral nerve injury induces calcium that is required for PP4c and to a lesser extent PP2a activity. PP4/2a are in turn needed to inhibit HDAC3 activity through dephosphorylation and to increase histone acetylation leading to DRG regenerative growth, including after a conditioning lesion. Lastly, HDAC3 serine 424 dephosphorylation, which requires PP4/2a, specifically controls DRG regenerative growth.

Combinatorial bioinformatics analysis of RNAseq, H3K9ac ChIPseq and HDAC3 protein–protein interactome suggests that HDAC3 is involved in the control of the regenerative gene expression programme

So far, we found that pharmacological or genetic HDAC3 inhibition (HDAC3mut) enhanced DRG neurite growth as well as histone H3K9 acetylation and that regeneration-competent SNA induces

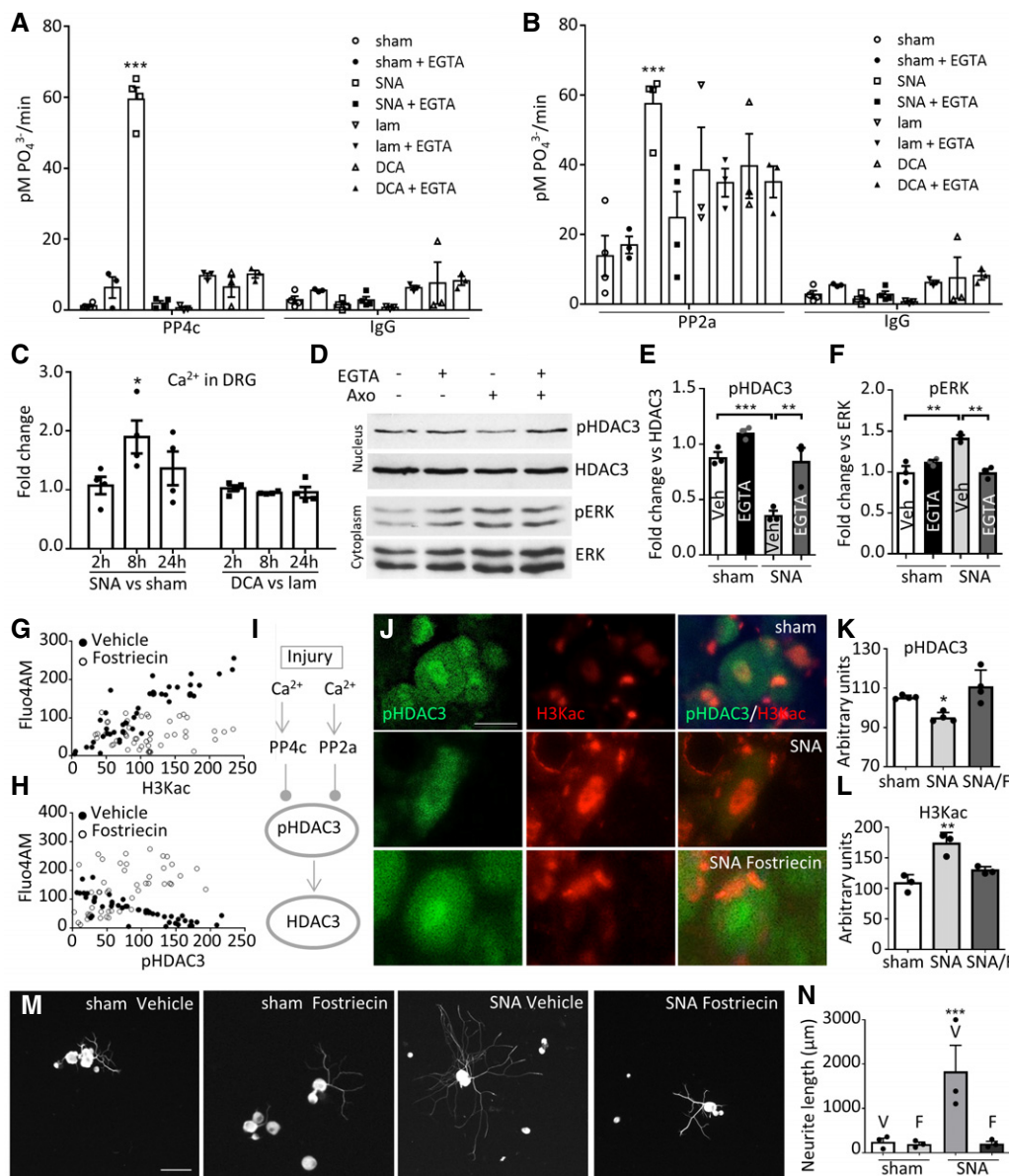


Figure 3. SNA-induced calcium regulates PP4/2 activity that in turn controls HDAC3 phosphorylation and DRG regenerative growth.

A, B PP4 and PP2 activities are induced after SNA but not DCA and are blocked by the calcium chelator EGTA. Data are expressed as mean ± s.e.m. *N* = 3–4 biological replicates. ****P* < 0.001 indicate significant difference versus sham or lam (two-way ANOVA followed by Bonferroni test).

C SNA but not DCA significantly enhances calcium levels in DRG. Data are expressed as mean ± s.e.m. *N* = 4 biological replicates. **P* < 0.05 indicate significant difference versus sham or lam (ANOVA followed by Bonferroni test).

D–F Immunoblotting of DRG homogenates shows that nerve injury-dependent nuclear HDAC3 dephosphorylation is reduced by the calcium scavenger EGTA upon *in vivo* delivery on the injured sciatic nerve (Axo = Axotomy). Cytoplasmic pERK levels are used as control of axotomy-dependent signalling. (E, F). Data are expressed as mean fold change of band intensity levels ± s.e.m. *N* = 3 biological replicates. ***P* < 0.01, ****P* < 0.001 indicate a significant difference (ANOVA followed by Bonferroni test).

G, H Significant Pearson’s correlations between calcium levels (Fluo4AM) and H3K9ac, *r*²: 0.7802 (G); or pHDAC3, *r*²: 0.6366 (H) in cultured DRG neurons after KCl. The Pearson correlations were disrupted by administration of Fostriecin (calcium and H3K9ac, *r*²: 0.0007; calcium and pHDAC3, *r*²: 0.3025). Data are expressed as single-cell fluorescence levels. *N* = 50 cells per condition from 4 biological replicates.

I Schematic pathway summarizing Ca²⁺- and PP4c- and PP2a-dependent HDAC3 dephosphorylation.

J–L Immunofluorescence (J) in DRG tissue sections 24 h after injury *in vivo* shows that the PP2a/PP4 inhibitor Fostriecin (F) inhibits the injury-induced decrease in pHDAC3 (K) and the increase in H3K9ac (L). Scale bar, 10 μm. (K, L). Data are expressed as mean fluorescence intensity in arbitrary units ± s.e.m. *N* = 3 (L) or 4 (K) biological replicates. **P* < 0.05; ***P* < 0.01 indicate significant difference versus sham (ANOVA followed by Bonferroni test).

M, N Pharmacological inhibition of PP2a/PP4 impairs conditioning-induced DRG neurite outgrowth *ex vivo* (12 h in culture). M. DRG neurite outgrowth (Tuj1-positive cells) 24 h after sham or sciatic nerve axotomy (SNA) prior to i.t. administration of vehicle (V) or Fostriecin (F) (240 μM). Scale bar, 100 μm. (N) Data are expressed as average neurite length per neuron ± s.e.m. *N* = 3 biological replicates per condition, technical triplicate. ****P* < 0.005 indicate significant difference versus sham/vehicle (one-way ANOVA followed by Bonferroni).

Source data are available online for this figure.

HDAC3 dephosphorylation and histone H3K9 acetylation in DRG neurons. Since H3K9ac depends on HDAC3 activity and is enriched at active promoters controlling gene expression, we investigated whether a regeneration-competent SNA would be associated with increased gene expression and H3K9ac enrichment. Therefore, we generated and combined RNAseq (Hervera *et al*, 2018) (GSE97090, <https://www.ncbi.nlm.nih.gov/geo/query/acc.cgi?acc=GSE97090>) with ChIPseq for H3K9ac (GSE108806, <https://www.ncbi.nlm.nih.gov/geo/query/acc.cgi?acc=GSE108806>) from sciatic DRGs 24 h after regenerative SNA vs. non-regenerative DCA. RNA sequencing identified 3,090 differentially regulated genes after SNA (1,503 upregulated and 1,587 downregulated), while after DCA, the gene expression programme was decreased by 3.7-fold (471 upregulated and 363 downregulated) ($P < 0.05$) (Fig 5A). H3K9ac ChIP revealed a significant enrichment of recovered DNA versus control IgG ChIP (Appendix Fig S2A). As expected, enrichment of H3K9ac after ChIP sequencing was prevalent at TSS, enhancers and gene bodies (Appendix Fig S2B). Genomewide analysis of H3K9ac revealed that H3K9ac occupancy increased specifically after SNA with respect to sham, but not after DCA with respect to laminectomy control (Fig 5B). This prompted us to assess the gene expression programme associated with changes in H3K9ac occupancy following SNA. To this end, we integrated ChIPseq and transcriptome data that allowed identifying 573 genes with increased H3K9ac occupancy after SNA (TSS \pm 1,000 bp plus gene body) associated with changes in gene expression (321 upregulated and 252 downregulated, $P < 0.05$), while only few genes showed changes in H3K9ac occupancy following DCA (Fig 5C and Dataset EV1). Increased H3K9ac occupancy was more highly correlated with upregulated genes (Fisher's exact $P = 1e-52$, Fig 5D), and decreased occupancy correlated with non-differentially expressed genes (Fisher's exact $P = 3e-15$, Fig 5D), supporting the interplay between enhanced histone acetylation and gene expression. It is worth noting that upon DCA, differentially expressed genes are significantly depleted for transcripts with changes in H3K9ac occupancy (Fig 5D). We next assessed whether these 321 upregulated SNA-responsive genes associated with increased H3K9ac occupancy were affected by non-regenerative DCA. Interestingly, we found that all of these transcripts were either downregulated or that their expression did not change (Fig 5E and Dataset EV1). The opposing activation of these H3K9ac-dependent genes between the two injury paradigms suggests that this might contribute to determining whether axonal regeneration is induced or not.

Next, we asked whether (i) the HDAC3 interactome (network of HDAC3 protein–protein interactions) could be regulated after injury and whether (ii) it shared key signalling pathways with those found to be associated with axonal regeneration. Therefore, we generated a HDAC3 interactome by FpClass analysis (Dataset EV2) and we evaluated how many of these HDAC3 interactors were differentially regulated after injury. Interestingly, about 23% of HDAC3 interactors were differentially regulated after SNA with 12.7% being upregulated and 9.8% downregulated, while only about 4% were differentially regulated after DCA (Appendix Fig S2C). GO analysis showed that the HDAC3 interactors differentially regulated after SNA are mainly involved in transcriptional regulation (Dataset EV3). Indeed, noteworthy, many of those HDAC3 interactors upregulated after SNA (Appendix Fig S2D and E, green) are regeneration-associated transcription factors such as Atf3, Jun, Fos, Cebpd, Klf6 and Hif1a. Some

of them showed opposite regulation after DCA (Appendix Fig S2D). Moreover, KEGG pathway analysis specifically revealed that HDAC3 interactors that are upregulated following SNA are enriched for signalling pathways associated with axonal regeneration, while this is not the case for the ones that are downregulated (Appendix Fig S3A and B and Dataset EV3). These pathways include MAPK, JAK-STAT3, neurotrophin, PI3K/AKT and cAMP signalling.

To identify possible upstream TFs that may be responsible for H3K9ac-dependent gene expression following SNA, we performed transcription factor enrichment analysis on the promoter of the identified 321 H3K9ac-regulated genes (Dataset EV4). Nineteen out of the identified 75 predicted TFs are found among the HDAC3 interactors which have been related to neuronal plasticity and regeneration (Appendix Fig S3C and D).

To probe the potential transcriptional and downstream signalling events associated with HDAC3 reduced activity upon regenerative injury, we built a protein–protein interaction network of the genes that were upregulated after SNA with increased H3K9ac occupancy and generated a hypothetical HDAC3-responsive signalling network (Fig 5F). The network displayed significant enrichment for signalling involved in the axonal regeneration programme including transcription factors, JAK-STAT, p53, neurotrophin, Wnt, MAPK signalling pathways and actin cytoskeleton regulation (Fig 5F and Dataset EV5).

Taken together, these data suggest that H3K9ac and HDAC3 may be involved in the control of the regenerative programme and that modulating HDAC3 activity might lead to synergistically targeting various signalling events that are associated with a regenerative phenotype. To verify this prediction, we investigated whether the *RGFP966*-dependent inhibition of HDAC3 following spinal injury (DCA) would enhance the expression level and promoter histone acetylation of key regenerative transcription factors and signalling pathways including the ones implied by our bioinformatics analysis (activated upon SNA but unchanged upon DCA) and summarized in the HDAC3-dependent signalling network in Fig 5F. We also tested where HDAC3 inhibition would be able to activate signalling pathways elicited by SNA and previously associated with axonal regeneration including JAK-STAT3, IGF1 and MYC. We delivered *RGFP966* intrathecally at the time of DCA, and 24 hours later, we tested the expression and H3K9ac occupancy of transcription factors and signalling molecules in DRG. We found increased H3K9 acetylation on ATF3, JUN, FOS, JAK1, STAT3 and IGF1R promoters in 966- vs. vehicle-treated DRG (Fig EV4A). Consistently, we found an increased protein expression for ATF3, JUN, pSTAT3, MYC, IGF1R and pERK in injured DRG neurons, however, not in non-neuronal DRG cells, 5 weeks following *RGFP966* treatment and SCI (Fig 6A and B), at a time where we also measured regeneration of DRG sensory neurons.

Taken together, these data suggest that inhibition of HDAC3 activity targets multiple signalling networks and pathways as predicted by bioinformatics analysis (Fig 5F), which are associated with a regenerative phenotype, likely by overcoming the repressive chromatin environment upon spinal injury.

Genetic and pharmacological inhibition of HDAC3 promotes DRG outgrowth *ex vivo* and axonal growth following spinal cord injury

Lastly, we investigated whether repression of HDAC3 activity by *in vivo* genetic or pharmacological inhibition would enhance DRG

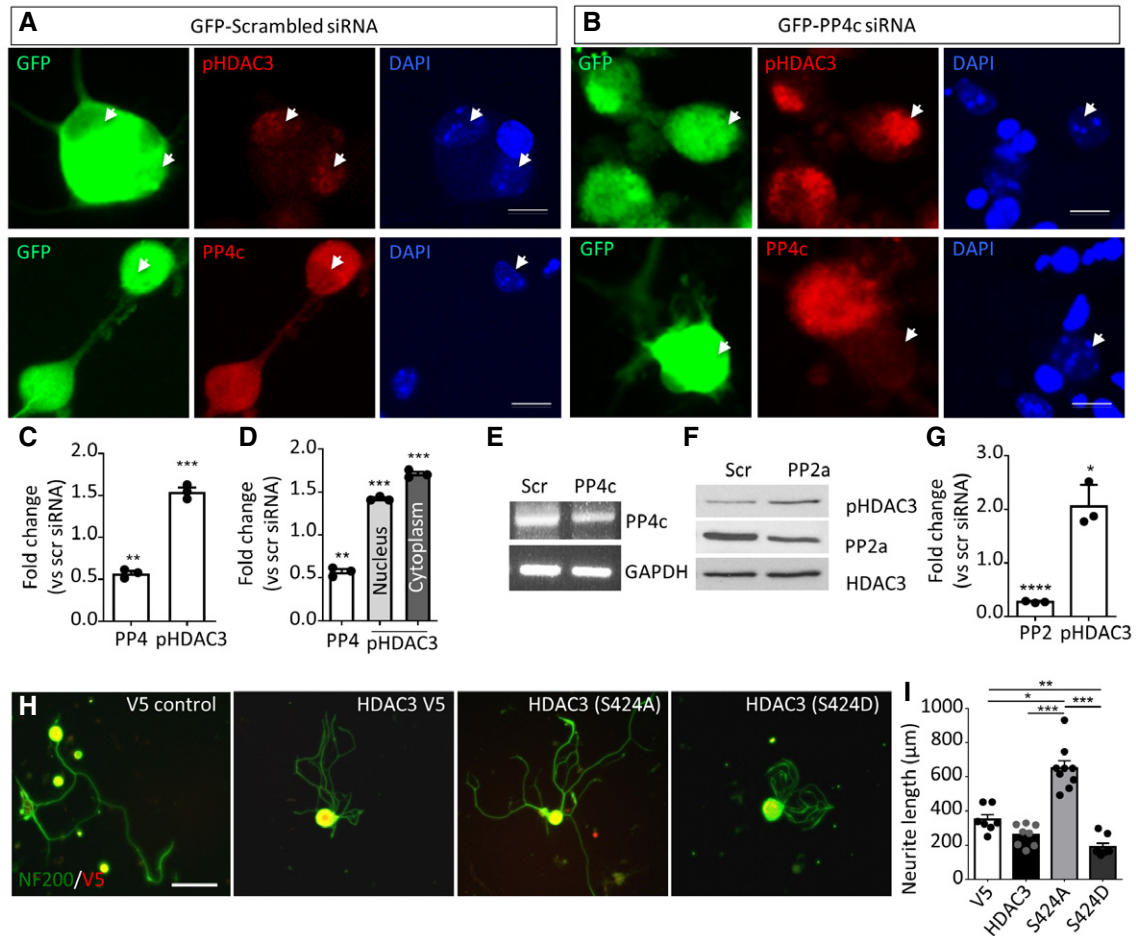


Figure 4. PP4c and PP2A dephosphorylate HDAC3 at Ser424, which is required for DRG outgrowth.

A–E PP4c gene silencing promotes HDAC3 phosphorylation in the presence of KCl (A–C, arrows), both in the nucleus and in the cytoplasm (D). Scale bar, 20 μm. (C,D) Data are expressed as mean fold change vs. scrambled (scr) siRNA of fluorescent intensity of pHDAC3 or PP4c in GFP-positive cells ± s.e.m. $N = 3$ biological replicates. $**P < 0.01$; $***P < 0.005$ indicate significant difference versus scrambled siRNA (Student's t -test). (E) PCR against PP4c demonstrates silencing of PP4c mRNA.

F, G PP2a gene silencing inhibits the KCl-induced dephosphorylation of HDAC3 as shown by immunoblotting of pHDAC3 (F). (G) Data are expressed as mean fold change of immunoblot band intensity ± s.e.m. $N = 3$ biological replicates $*P < 0.05$; $****P < 0.001$ indicate significant difference versus control siRNA (Student's t -test).

H, I Genetic modification of activity-dependent phosphorylation of serine 424 of HDAC3 affects DRG neurite outgrowth. (H) DRG neurite outgrowth after transfection of control (V5 control), WT HDAC3-V5, phospho-dead HDAC3 (S424A)-V5 or phospho-mimetic HDAC3 (S424D)-V5 and after 24 h in culture. Scale bar, 50 μm. (I) Data are expressed as mean ± s.e.m. $N = 8–9$ biological replicates, approximately 35 V5-positive cells each. $*P < 0.05$, $**P < 0.01$, $***P < 0.005$ indicate significant difference (one-way ANOVA followed by Bonferroni).

Source data are available online for this figure.

regenerative growth across the inhibitory spinal cord environment. Therefore, we aimed to inhibit HDAC3 activity in DRG neurons before a spinal cord injury. AAV-HDAC3mut-V5 or an AAV-V5 control virus was injected into the sciatic nerve of adult mice 4 weeks prior to a T9 spinal cord dorsal column crush, which preferentially severs ascending sensory fibres originating from the DRG. Five days before sacrificing the animals, at day 28 post-injury, the fluorescent axonal tracer dextran was injected in the sciatic nerve to examine axonal growth in the spinal cord. An average of $88 \pm 1.9\%$ for the control and $85 \pm 1.6\%$ for the HDAC3mut of dextran-positive cells showed also positive signal for V5 transduction (Appendix Fig S4A). Data analysis revealed that inhibition of HDAC3 activity with HDAC3mut promotes significant axonal

growth (Fig 7A, B, K and L, control for spared axons, Appendix Fig S4B), and it enhances histone acetylation in transduced DRG neurons (Fig 7C–F, Appendix Fig S4D). Furthermore, we observed that axons of mice transduced with HDAC3mut express pre-synaptic vGlut1 as shown by dextran/vGlut1 co-labelling (Fig 7G–J). In support of a specific role for AAV-HDAC3mut in neurite outgrowth of DRG neurons, we found that intrathecal delivery of AAV-HDAC3mut significantly enhanced neurite outgrowth in *ex vivo* cultured DRG neurons to a higher degree than a control virus or a conditioning lesion (Fig EV4B and C). Taken together, these data show that inhibition of HDAC3 activity can enhance the regenerative potential of DRG neurons. Next, we tested whether intrathecal administration of *RGFP966* through osmotic minipumps could also

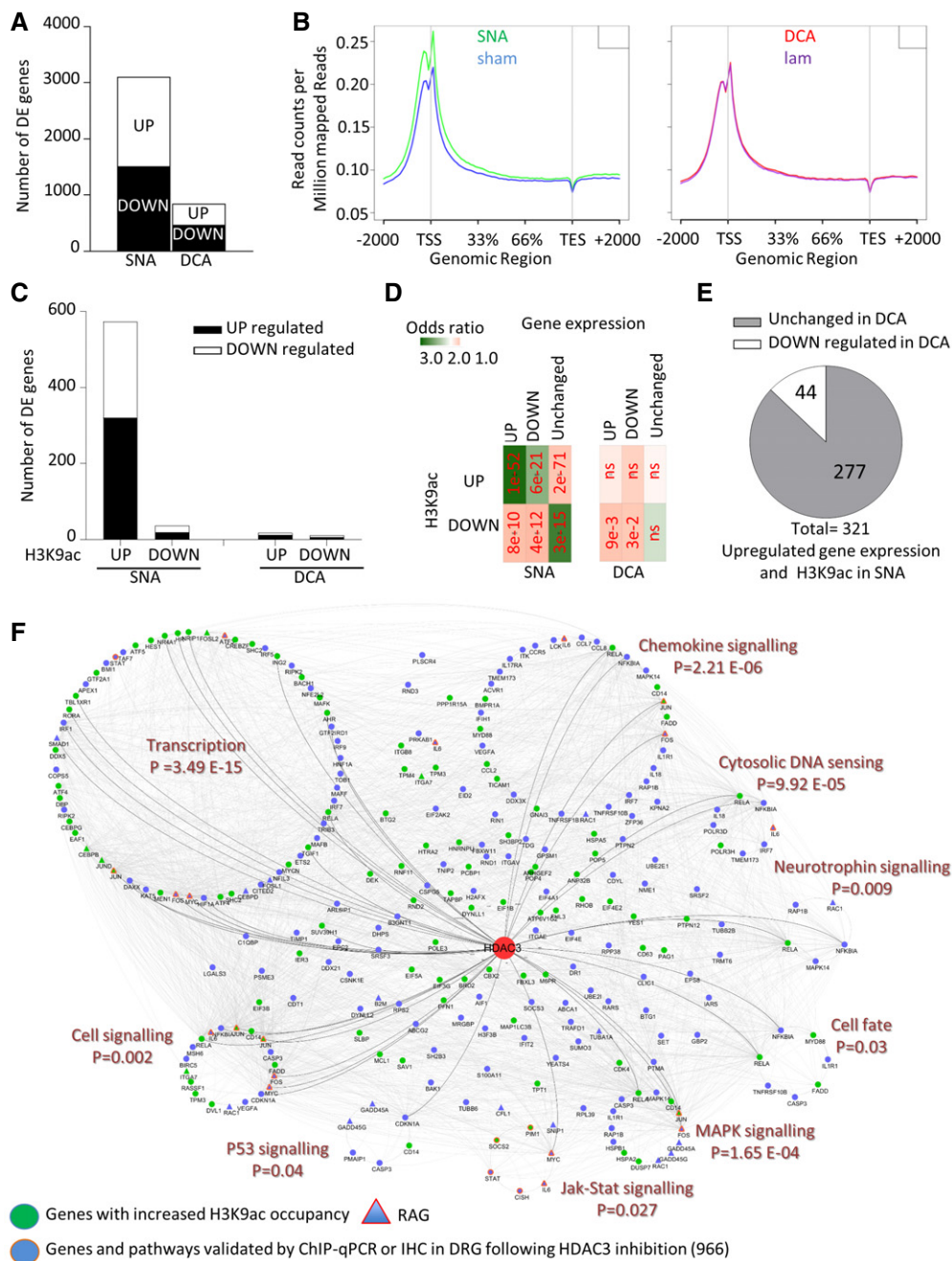


Figure 5. H3K9ac ChIPseq and HDAC3 interactome signalling network.

- A The graph shows the number of differentially expressed (DE) genes 24 h following SNA or DCA compared to their respective controls.
- B RNAseq read counts show differential occupancy of H3K9ac on specific gene regions, including an increased occupancy close to the transcriptional start site (TSS) after SNA only, when compared to corresponding controls.
- C Bar graph shows the number of genes that are upregulated or downregulated following SNA or DCA (RNAseq) with an increased or decreased H3K9ac occupancy (ChIPseq), respectively.
- D Odds ratio analysis of the enrichment/depletion of genes with differential H3K9ac occupancy across each upregulated and downregulated gene cluster in (C); the numbers in red represent the *P* value given by Fisher's exact test (ns = not significant).
- E Out of the 321 upregulated genes associated with increased H3K9ac upon SNA, the majority does not show a change in expression following DCA (grey), while some of them are downregulated (white).
- F Cytoscape visualization of the protein network resulting from HDAC3 interactome and H3K9ac ChIPseq and RNaseq upon SNA. The signalling network was created by combining the protein interactome of HDAC3- and H3K9ac-dependent genes with increased gene expression upon SNA. HDAC3 is in red at the centre of the network. The line thickness is proportional to the interaction score. Highlighted in orange circles are the validated pathways and targets via IHC (Fig 6) or ChIP-qPCR (Fig EV4), and regeneration-associated genes (RAG) are highlighted in orange triangles.

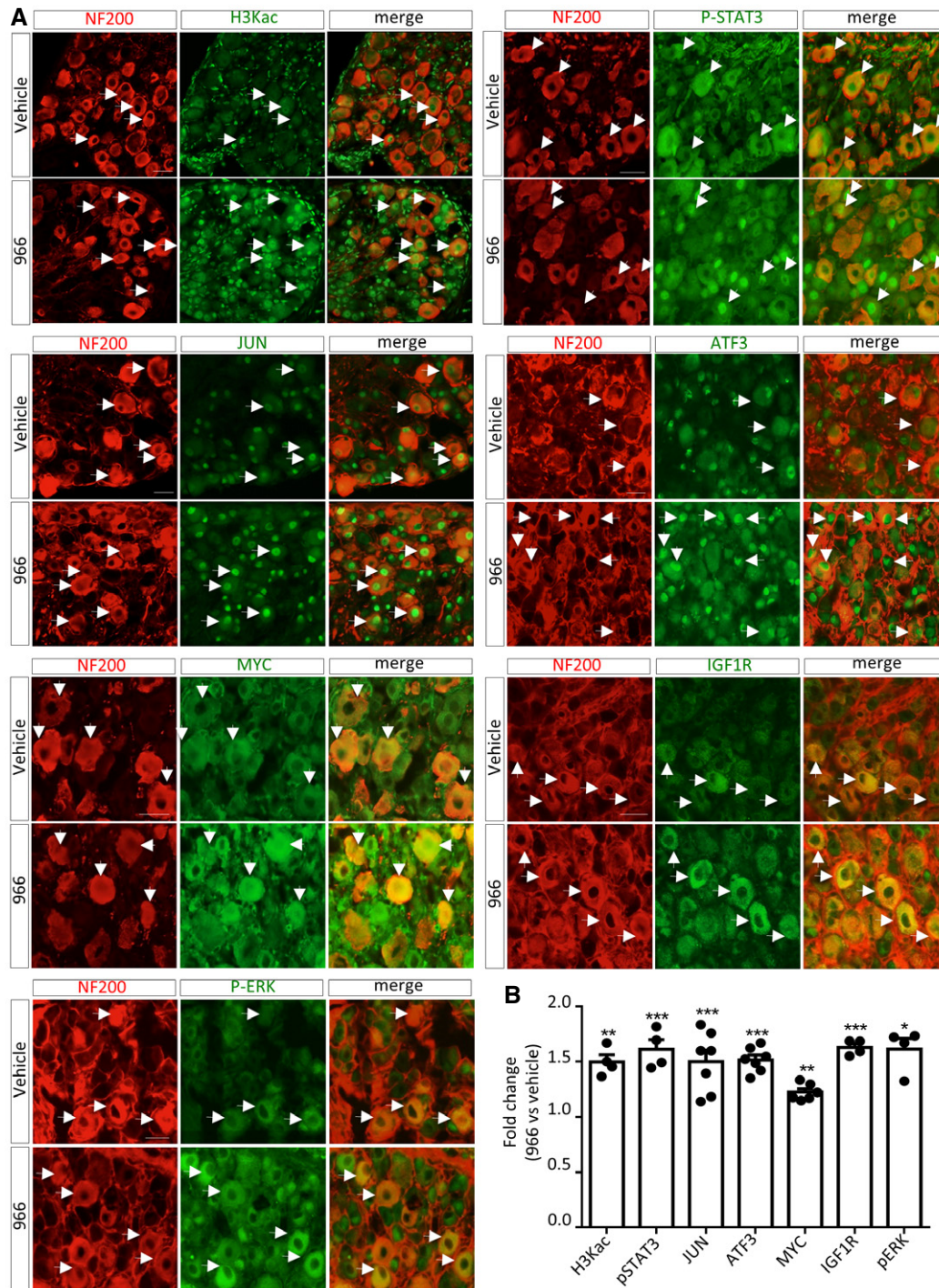


Figure 6. Intrathecal pharmacological inhibition of HDAC3 activity promotes H3K9ac and RAG expression in DRG neurons after spinal cord injury.

A, B (A) Co-immunofluorescence of anti-neuronal and anti-regeneration-associated proteins in DRG following SCI and treatment with 966 or vehicle. Shown is increased protein expression for regeneration-associated targets in NF200-positive DRG neurons (arrows) after 966 treatment (5 weeks following SCI). Scale bar, 50 μ m. (B) Data are expressed as fold change of fluorescence intensity in NF200⁺ cells, 966 versus vehicle \pm s.e.m. $N = 4-7$ biological replicates * $P < 0.05$, ** $P < 0.01$, *** $P < 0.005$ indicate significant difference versus vehicle (Student's t -test).

enhance growth of DRG sensory axons after spinal cord injury in a model of dorsal hemisection in the adult mouse. *RGFP966* or vehicle was delivered for 2 weeks post-injury through an intrathecal

catheter placed in proximity to the lesion site from the time of the spinal injury. Axonal labelling of dextran-traced DRG sensory ascending fibres into and past the lesion was evaluated together

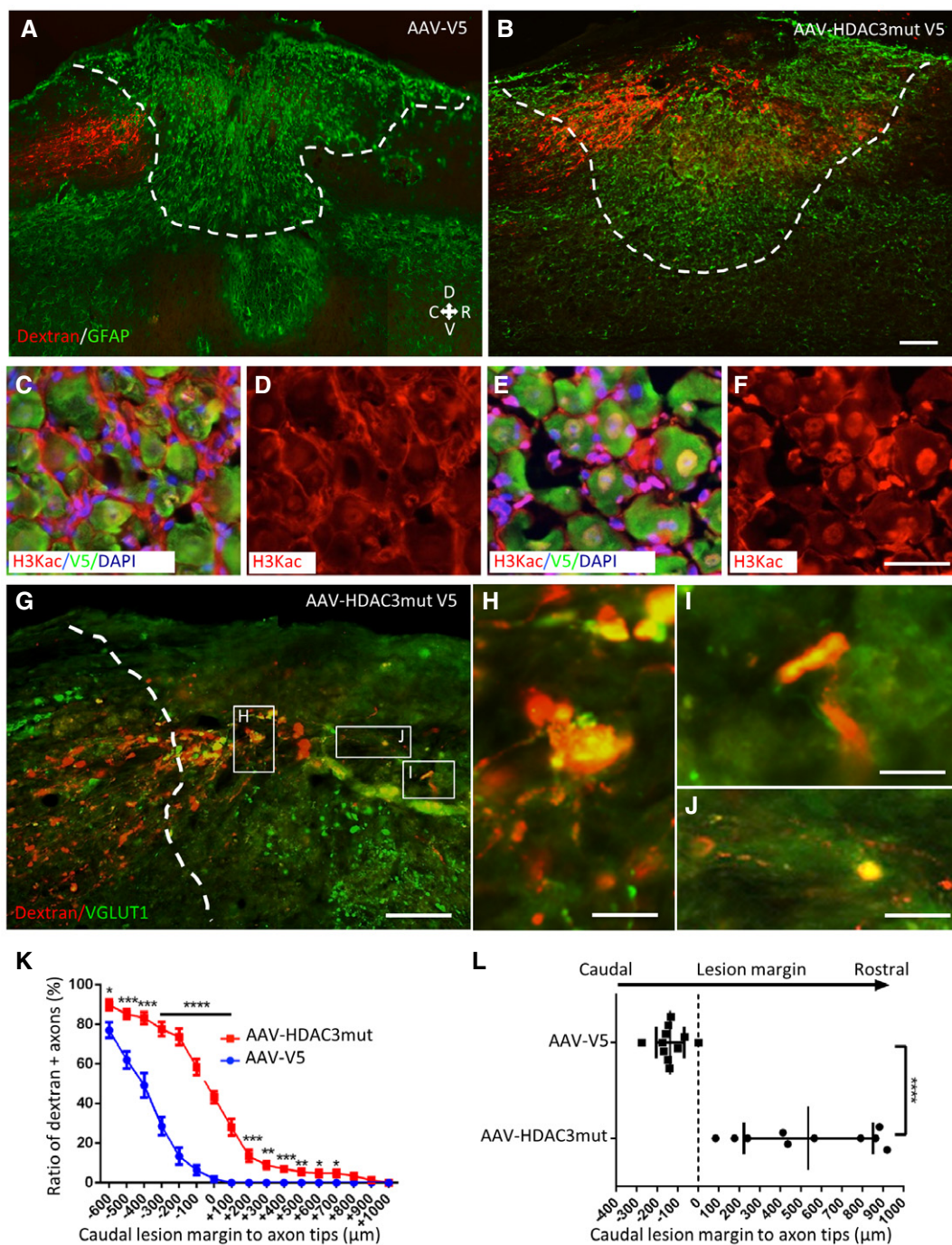


Figure 7. Genetic inactivation of HDAC3 deacetylase activity with HDAC3 dead mutant promotes DRG regenerative growth *in vivo* after SCI.

A, B AAV-HDAC3 mutant (Y298H; dominant negative deacetylase inactive) promoted DRG regenerative growth after spinal cord injury vs. AAV-V5 control (injected 5 weeks prior to SCI in the sciatic nerve bilaterally) as shown by dextran-red-traced axons across and beyond the lesion site (GFAP, green) (dotted lines denote the rostral and caudal margins of the scar around the lesion). Scale bar, (A, B) 200 μm.

C–F Immunofluorescence for H3K9ac. AAV-HDAC3 mutant induced upregulation of H3K9ac *in vivo* in DRG neurons, but not in surrounding nuclei of satellite cells. Scale bar, (C–F) 50 μm.

G–J New synaptic formations (VGLut1⁺) from regrowing axons are shown beyond the lesion site after injection of AAV-HDAC3mut. (G) Scale bar 200 μm, (H–J) high-magnification insets depict co-localization of dextran and vGlut1 staining. Scale bar 50 μm.

K, L Quantification of dextran-positive axons shows that AAV-HDAC3mut promotes DRG regenerative growth across and beyond the spinal lesion site. Data are expressed as percentage of dextran⁺ axons at each distance vs. dextran⁺ axons at –700 μm from the lesion margin (K) or distance from the caudal margin of the lesion to the most rostral dextran⁺ axon tip for each animal (L). N = 10 animals per condition, ± s.e.m. *P < 0.05, **P < 0.01, ***P < 0.005, ****P < 0.001 indicate a significant difference (ANOVA followed by Bonferroni test).

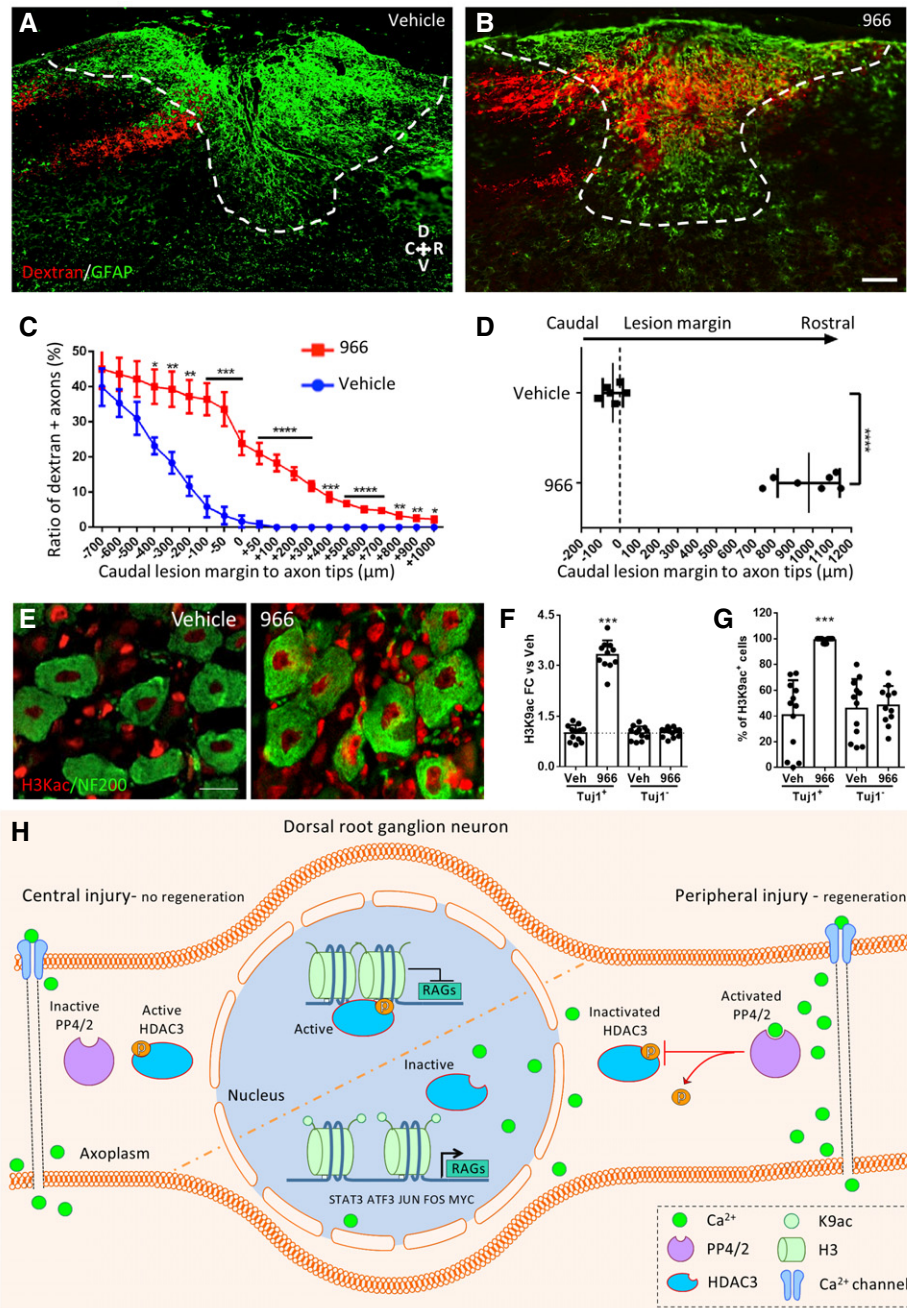


Figure 8. Pharmacological inhibition of HDAC3 promotes DRG regenerative growth.

A, B Intrathecally administered RGFP966 (966) through osmotic minipump for 14 days promoted DRG regenerative axonal growth after spinal cord injury as shown by dextran-red-traced axons across and beyond the lesion site (GFAP, green) (dotted lines denote the rostral and caudal margins of the scar around the lesion). Scale bar, 200 μm.

C, D Quantification of axonal regeneration shows dextran axonal labelling across and beyond the spinal lesion site. Data are expressed as ratio of dextran+ axons vs. dextran+ axons at -700 μm from the lesion site ± s.e.m (C) or distance from the caudal margin of the lesion to the last dextran+ axon tip (D). N = 6–10 animals per condition. *P < 0.05, **P < 0.01, ***P < 0.005, ****P < 0.001 indicate a significant difference (ANOVA followed by Bonferroni test).

E Immunofluorescence for H3K9ac and Neurofilament 200 (NF200) shows upregulated H3K9ac *in vivo* in DRG neurons after 966. Scale bar, 50 μm.

F, G Data are expressed as fold change of fluorescence intensity mean levels (F) or % of H3K9ac+ cells (G) (H3K9ac+ threshold was set at the mean intensity level of vehicle-treated animals, and DAPI counterstaining was used to label nuclei from NF200+ or NF200- cells) vs. veh ± s.e.m. N = 11–12 biological replicates. ***P < 0.005 indicate a significant difference vs. respective Veh (ANOVA followed by Bonferroni test).

H Summary diagram: following central nervous system (CNS) spinal injury, protein phosphatase 4/2 activity is not induced since calcium levels remain unchanged compared to uninjured conditions. HDAC3 remains phosphorylated and occupies deacetylated chromatin contributing to its compaction-inhibiting gene expression. Following peripheral nervous system (PNS) sciatic injury, protein phosphatase 4/2 activity is induced by calcium. HDAC3 is dephosphorylated leading to its inhibition and release from chromatin sites contributing to increase in histone acetylation and in the expression of regeneration-associated genes (RAGs).

with the measurement of the glial scar 5 weeks after SCI. Importantly, we found that mice treated with RGFP966 showed increased growth of DRG sensory axons (Fig 8A–D), and as expected, RGFP966 led to significant enhancement in histone acetylation in DRG (Fig 8E and G), but not in non-neuronal cells. We included in our analysis only spinal cords without sparing of axon fibres as shown by cross sections of cords far rostral to the lesion site (Appendix Fig S4C). Similarly, intrathecal delivery of the HDAC3 inhibitor RGFP966 triggered significant neurite outgrowth in *ex vivo* cultured DRG neurons compared to vehicle on both growth-permissive and inhibitory substrates (Fig EV4D and E). Importantly, the glial scar and anti-CD11b immunoreactivity around the injury site remained unaffected in RGFP966- versus vehicle-treated mice (Fig EV5).

Discussion

Our data propose calcium-dependent activation of PP4c and to a lesser extent of PP2a leading to dephosphorylation of HDAC3 as a novel molecular mechanism that discriminates between axonal regeneration versus regenerative failure in DRG sensory neurons. Specifically, we found that calcium increases in DRG following a regeneration-competent sciatic but not a regeneration-incompetent spinal injury to activate PP4c that is required for HDAC3 dephosphorylation. While PP4 has been shown to play a role in phagocytic clearance of degenerating axons in *Drosophila* (Winfree et al, 2017), its role in axonal regeneration remained unexplored so far. Similarly, while calcium has been linked to the activation of multiple signalling pathways in injured axons, it was previously unknown whether a central spinal lesion associated with regenerative failure would fail to trigger significant increases in calcium in the DRG cell bodies. Here, we found that calcium, which is required for PP4/2 activation, is induced in DRG following peripheral regenerative axotomy only.

HDAC3 dephosphorylation inhibits HDAC3 activity following a sciatic nerve injury, while it remains elevated after a non-regenerative central spinal injury. Reduced HDAC3 activity in turn allows for increased histone acetylation and regenerative gene expression in DRG. Indeed, inhibition of PP4/2 activity restricts DRG regenerative growth while inhibition of HDAC3 phosphorylation or activity leads to an enhancement in DRG neurite outgrowth on both growth-permissive and inhibitory substrates. Subsequent bioinformatics analysis integrating the HDAC3 protein–protein interaction databases combined with DRG *ex vivo* H3K9ac ChIPseq and RNAseq after a central spinal versus peripheral sciatic lesion further supported a role of HDAC3 in restricting the regeneration programme. Additionally, we found that *in vivo* HDAC3 pharmacological inhibition following spinal cord injury promotes the promoter acetylation and protein expression in DRG neurons of several regeneration-associated genes belonging to signalling pathways that were identified by our combinatorial bioinformatics analysis. They include several transcription factors such as JUN, MYC, STAT3, ATF3 and FOS within key signalling pathways such as MAPK, insulin and JAK-STAT.

Ultimately, the genetic or pharmacological inhibition of HDAC3 led to significant DRG regenerative growth after spinal cord injury.

While a direct role for HDAC3 in axonal regeneration had not been reported so far, a recent study found that HDAC3 plays also a role in the control of Schwann cell-dependent myelination in the peripheral nerve, where pharmacological inhibition of HDAC3 with RGFP966 promotes remyelination and functional recovery in the injured peripheral nervous system (He et al, 2018).

It has also been shown that HDAC3 might control the expression of immune-related gene targets in inflammatory models of SCI such as contusion injuries, where systemic pharmacological HDAC3 inhibition with RGFP966 was followed by improved functional recovery (Kuboyama et al, 2017). However, HDAC3 systemic pharmacological inhibition did not alter the extent of the CD11b-positive inflammatory response around the injury site after spinal contusion (Kuboyama et al, 2017), in line with what we found here through intrathecal administration of RGFP966 after spinal dorsal hemisection. The same authors observed that systemic administration of RGFP966 did not affect neurite outgrowth of DRG neurons at 48 hours in culture (Kuboyama et al, 2017). This is in contrast to our findings showing that intrathecal delivery of RGFP966 promotes DRG regenerative growth in culture. These data were supported by enhanced DRG neurite outgrowth following genetic HDAC3 inhibition. The different route of administration and the timing of when neurite outgrowth has been measured might explain this discrepancy.

Our data also suggest that axonal regeneration of sensory neurons does not depend upon the generalized inhibition of HDACs or of DNA methyltransferases, as modifying the activity of the various histone-modifying enzymes within our screen had no effect on DRG regenerative growth. This is in line with the poor or absent representation of DNA methylation on gene regulatory regions of DRG after nerve or spinal injury (Lindner et al, 2014) and the absent or limited regenerative potential of generalized HDAC inhibition after optic nerve or spinal injury (Finelli et al, 2013; Gaub et al, 2011). In fact, the biological effect of the inhibition of specific HDACs or classes of HDACs is very heterogeneous and at times very different from one another in terms of both gene expression and cell phenotype. These include diverse effects on a variety of cellular processes, such as cell cycle regulation, stem cell differentiation, development and memory and brain function (Bose et al, 2014). This is likely because individual HDACs differently influence the epigenetic and gene regulatory environment by interacting with a different array of cell-specific transcription factors, histone-modifying enzymes and additional epigenetic modifiers such as REST and NCOR among others. Indeed, our data show that HDAC3 inhibition contributes to a favourable transcriptional environment that allows regenerative growth while other HDAC inhibitors do not.

It is in fact likely that specific signalling pathways shape the transcriptional environment of DRG neurons that determine whether axonal regeneration succeeds or fails. This will restrict the regrowth programme after spinal cord injury, and in contrast, it will work as a central regulatory hub for regenerative signalling following DRG sensory axonal injury.

We previously discovered that HATs CBP/p300 and P/CAF form a transcriptional complex with the transcription factor p53 in primary neurons to enhance promoter accessibility of regenerative genes via an active chromatin state on select regenerative gene promoters (Di Giovanni et al, 2006; Gaub et al, 2010; Tedeschi et al, 2009). This was observed both *in vitro* and *in vivo*, where the p53-

CBP/p300-P/CAF transcriptional complex was essential for neurite outgrowth and therefore activated during the axonal regenerative programme (Gaub *et al*, 2010; Tedeschi *et al*, 2009), which is dependent upon an active p53 including after SCI (Floriddia *et al*, 2012). In addition, we have recently found that viral overexpression of the histone acetyltransferase p300 can promote axonal regeneration of the optic nerve after optic nerve crush (Gaub *et al*, 2011), while overexpression of P/CAF promotes regeneration after spinal cord injury suggesting that both transcriptional and acetylation-dependent epigenetic mechanisms can directly sustain axonal regeneration in these sensory neurons. Studies by others have recently shown that p300 forms a complex with the transcription factor SMAD1 in DRG after a conditioning lesion (Barlow, 1992). It is therefore possible that post-injury calcium levels that regulate PP4c activity determine whether active or inactive HDAC3 restricts or allows the accessibility of regenerative transcriptional complexes such as p300 and P/CAF as well as with the associated transcription factors, including SMAD1 and p53 to specific promoters.

Although the axonal injury-dependent regulatory mechanism upon HDAC3 does not involve nuclear–cytoplasmic translocation, but rather PP4 and calcium-dependent HDAC3 dephosphorylation, this is conceptually in line with the reported injury- and calcium-dependent cytoplasmic export of HDAC5, which enhances axonal regeneration in the PNS (Cho *et al*, 2013). Interestingly, since HDAC5 does not seem to have catalytic activity (Lahm *et al*, 2007), it is possible that peripheral nerve regeneration may be controlled via interaction between HDAC5 and HDAC3 activity. However, whether HDAC5 plays a role in discriminating between regenerative success and failure such as following spinal cord injury was not investigated.

Since whole DRGs contain both neurons and satellite cells, the development of combinatorial single-cell RNAseq and ChIPseq will hopefully soon allow studying genetic and epigenetic changes specifically in neuronal populations, adding further specificity to unbiased molecular screenings. However, immune cell infiltration into the ganglion induced by a peripheral nerve typically occurs at a much later time points (peaking at 7–14 days after lesion; Kim & Moalem-Taylor, 2011; Kim *et al*, 2011) than the one used in this study (24 h), where we did not observe any accumulation of inflammatory cells in sciatic ganglia.

Taken together, our findings show a novel mechanism for the regulation of the differential regenerative ability between regeneration-competent peripheral versus regeneration-incompetent central axonal injury. We found that (i) calcium-dependent activation of PP4 leads to HDAC3 dephosphorylation causing in turn HDAC3 enzymatic inhibition; (ii) HDAC3 restricts the axonal regeneration programme; and (iii) pharmacological or genetic inhibition of HDAC3 activity promotes regenerative signalling and (iv) enhances the axonal growth state of sensory neurons partially overcoming regenerative failure after SCI.

Materials and Methods

Mice

Animal work was carried out in accordance with regulations of the UK Home Office. Wild-type C57Bl6/J (Harlan) mice ranging from 6

to 8 weeks of age were used for all experiments. Male and female were used in a 50–50% basis for each study. Each animal was randomly assigned to an experimental group. For all surgeries, mice were anaesthetized with isoflurane (5% induction 2% maintenance) and a mixture of buprenorphine (0.1 mg/kg) and carprofen (5 mg/kg) was administered peri-operatively as analgesic. Animals outside the 6–8 week or 15–30 g range were excluded for the use in any study. Animals wounded or with clear signs of distress were also excluded. All animal procedures were approved by Imperial College London Ethics Committee and were performed in accordance with the UK Animals Scientific Procedures Act (1986).

Compounds

RGFP233, 933 and 966 were received from Repligen. GW376713X (13X), GSK1786269A (69A), GSK1210151A (51A), GSK503 (503), GSK2961917A (17A), GSK2668977A (J4), GSK2801 (801), GSK484 (484), GSK2924467A (67A) and GSK2980071B (71B) were obtained from a collaboration through an MTA with GSK. EGTA and KCl were purchased from Sigma and Fostriecin from Cayman. For each group treated with a drug, the respective control group received the same volume of vehicle.

Dorsal column axotomy

Surgeries were performed as previously reported (Floriddia *et al*, 2012). Briefly, mice were anaesthetized and a T9 laminectomy was performed (~20 mm from the sciatic DRGs), and the dura mater was removed, taking care of not damaging the spinal cord. A dorsal hemisection until the central canal was performed with fine forceps (FST). For the control laminectomy surgery, the dura mater was removed but the dorsal hemisection was not performed.

Sciatic nerve axotomy

Briefly, sciatic nerve lesion experiments were performed under isoflurane anaesthesia. The biceps femoris and the gluteus superficialis were separated by blunt dissection, and sciatic nerve was exposed. Sciatic injury was performed by a sharp axotomy with iridectomy scissors (FST). Sham-operated mice that underwent exposure of the sciatic nerve without axotomy were used as surgery controls.

Dorsal root ganglia (DRG) cell culture

Adult DRGs were dissected and collected in Hank's balanced salt solution (HBSS) on ice. DRGs were transferred to a digestion solution (5 mg/ml Dispase II (Sigma), 2.5 mg/ml Collagenase Type II (Worthington) in DMEM (Invitrogen)) and incubated at 37°C for 45 min with occasional mixing. Thereafter, DRGs were transferred to media containing 10% heat-inactivated FBS (Invitrogen) and 1X B27 (Invitrogen) in DMEM:F12 (Invitrogen) mix and were manually dissociated by pipetting until no remaining clumps of DRGs were observed. Next, single cells were spun down, resuspended in media containing 1X B27 and penicillin/streptomycin in DMEM:F12 mix and plated at 3500/coverslip. The culture was maintained in a humidified atmosphere of 5% CO₂ in air at 37°C. Cells were allowed to grow for 12 h, unless otherwise specified, in culture before fixation.

Ex vivo DRG cell culture

Animals underwent intrathecal injections of 5 μ L RGFP966 (10 or 100 μ M), Fostriecin (240 μ M) or vehicle (5% DMSO in 0.9% saline) or 2 μ l of AAV1 (control or HDAC3mut) into cerebrospinal fluid (CSF) between L5 and L6 laminae, or alternatively, 100 μ l of EGTA 10 mM or vehicle (0.9% saline) was applied to sciatic nerve before performing sham or SNA surgeries as above mentioned. Twenty-four hours later, sciatic bilateral DRGs were dissociated and plated following the above protocol.

Calcium imaging

Dorsal root ganglia primary cells were cultured for 12 h following standard protocol. Cells were washed with Ringer solution and loaded with Fluo-4AM (2 μ M, Thermo Scientific) diluted in Ringer solution, after 30-min incubation at RT protected from light. Cells were washed, and KCl-Ringer solution was applied (40 mM KCl). For Fostriecin-treated cultures, cells were pre-treated for 30 min with vehicle (1% DMSO) or Fostriecin (200 nM) before KCl administration. Cells were monitored for KCl-induced Fluo-4AM fluorescence increases. Cells were then fixed, such that the KCl-induced increase in fluorescence was frozen, and subsequently stained for H3K9ac, pHDAC3 or HDAC3. Correlation between Fluo-4AM and immunostaining levels was quantified and plotted.

PP4/PP2A activity

Protein phosphatase 4c and 2A activities were measured by measuring phosphatase activity (PP2A phosphatase activity kit, Millipore, CA, USA) on DRGs after central and peripheral injury prior to PP4 or PP2A immunoprecipitation. Briefly, sciatic DRGs were extracted 24 h after surgery, protein lysates were obtained with 1 litre of imidazole buffer (20 mM imidazole-HCl, 2 mM EDTA, 2 mM EGTA, pH 7.0 with 10 μ g/ml each of aprotinin leupeptin, pepstatin, 1 mM benzamidine and 1 mM PMSF) per 25 g of tissue, homogenized with micropestles on ice and centrifuged at 2,000 g for 5 minutes at 4°C. Protein lysate concentration was measured by BCA, and 100 μ g of protein was used for each reaction, together with 4 μ g of PP2A (Millipore, CA, USA), PP4 (PPX, Santa Cruz, CA, USA) antibodies or Mouse IgG (Millipore, CA, USA). Samples were processed following the kit instructions, and activity of samples was then measured in an Infinite M200 Pro Microplate Reader (Tecan) at 650 nm according to the manufacturer's guidelines.

Ex vivo calcium assay

Dorsal root ganglia was dissected 24 h following sham, SNA, laminectomy or DCA. Each dissected DRG was immediately transferred into pre-chilled Eppendorf tube on dry ice and flash-frozen per collection. Samples homogenates were employed for calcium measurement by using the Calcium Detection Assay Kit (Abcam). In particular, sciatic DRG from 3 mice per replicate was homogenized with a sonicator in 120 μ l Calcium Assay Buffer on ice and the collected supernatant was used for calcium detection on a microplate reader (OD575 nm) following the manufacturer's protocol. Calcium concentration was normalized by protein concentration of

each sample after BCA assay (4 biological replicates for each condition).

PP4/PP2A RNA silencing

Following DRG dissection and dissociation, cells were washed twice with HBSS and transfected with a mixture of a GFP and siRNA plasmids mixture using Amaxa 4D-Nucleofector Kit (Lonza). Briefly, 50,000 DRG cells per reaction were resuspended with 20 μ l Nucleocuvette Strip (16.4 μ l nucleofector solution, 3.6 μ l Supplement) and 0.4 μ g pmaxGFP mixed with 6 pmol of control, PP2a or PP4c siRNAs (Santa Cruz) were applied per reaction. After nucleofection, cuvettes were incubated 10 min at RT and cells were resuspended with pre-warmed DRG medium. 25,000 cells were plated per coverslip for 72 h. Due to the lack of efficient antibodies against PP4, verification of silencing was performed via immunocytochemistry as described below and PCR using the primers provided in the kit (Santa Cruz, sc-39203-PR). For PP2a silencing, verification of silencing was performed via immunoblotting as described below.

Mutant HDAC3 variant transfection in DRG cultures

HDAC3 constructs were cloned on a pAAVIREShrGFP backbone (Agilent). FLAG tag, the IRES element and the GFP were removed from the original backbone via restriction on the BamHI site in the MCS and the second Kpn1 site after GFP and were replaced with either the V5 tag MW87 (empty vector), HDAC3 (seq. accession number NM_014111) + V5 tag (wild-type HDAC3), HDAC3 S424A + V5 tag or HDAC3 S424D + V5 tag. Briefly, DRGs were dissected and dissociated as mentioned previously, and cells pellets were resuspended after digestion with an Opti-MEM (Invitrogen) solution containing 10 μ l/ml of Lipofectamine 2000 (Invitrogen) and 6.25 μ g/ml of DNA. Cells were allowed 3 h for the transfection, and then, transfection solution was replaced with normal DRG medium. Cells were fixed after 24 h.

RNA sequencing

Sciatic DRGs (3 biological replicates, pool of 2 mice/replicate) were extracted 24 h after sham, sciatic nerve axotomy, laminectomy or dorsal column axotomy surgeries (surgeries were performed as described above), and RNAseq was performed and analysed as we previously described (Hervera *et al*, 2018). Sequence reads were aligned to the mm10 mouse reference genome sequence using TopHat version 2.0.12 running Bowtie 2-2.2.3. Gene structure annotations corresponding to the Ensembl annotation of the mm10 genome sequence were used to build a transcriptome index and provided to TopHat during the alignment step. The aligned reads were sorted using Samtools-0.1.19, and then, read counts per gene were obtained from mapped reads using HTSeq-0.6.1. edgeR version 3.8.6 (using limma-3.22.7) in R-3.1.1 was used to identify differentially expressed genes. Following the procedures described in the edgeR documentation, read count tables were loaded into R. GC-content bias was controlled for using full quantile normalization in EDASeq-2.0.0 running in R-3.1.1. EDASeq was also used to generate quality-checking figures before and after this normalization. Differential expression testing was performed on the normalized output

from EDASeq using edgeR. Read-level quality checking was performed using fastqc-0.10.1 and the fastqc-aggregator (https://github.com/staciaw/fastqc_aggregator), and gene-level quality checking was performed using RSeQC-2.6.1. The cut-off criteria for the differentially expressed (DE) genes were set at FDR < 0.05.

H3K9ac ChIP sequencing

Sciatic DRGs (2 biological replicates, pool of 20 mice/replicate) were extracted as above, 24 h after sham, sciatic nerve axotomy, laminectomy or dorsal column axotomy surgeries. Chromatin IP was performed according to our previously published protocol¹⁴ with a few adjustments. Briefly, DRG pellets were crushed using an automatic pestle and chemically cross-linked with a 1% formaldehyde solution containing 50 mM HEPES-KOH pH7.5, 100 mM NaCl, 1 mM EDTA and 0.5 mM EDTA, for 15 min at room temperature. Nuclear extracts were then sonicated for 30 min using a Bioruptor (Diagenode), and successful chromatin shearing (200–800 bp) was confirmed by agarose gel analysis. Immunoprecipitation was performed overnight with Protein G Dynabeads (Invitrogen) bound to 10 µg of H3K9ac antibody (Ab10812, Abcam). After washing, elution and reverse cross-linking, DNA was treated with RNase A and Proteinase K and purified using Qiagen PCR purification columns. The concentration of the recovered DNA was quantified with PicoGreen assay and the enrichment of the immunoprecipitate calculated with respect to the input and IgG. Library preparation was performed using the NEBNext Ultra DNA Library Prep Kit from Illumina (New England Biolabs) following the manufacturer's protocol. Briefly, 30 ng of input and IP DNA were end-repaired and adaptor-ligated, using a dilution of 1:10 of adaptors. Samples were cleaned to remove unligated adaptors, and size selection was performed to select and enrich fragments of 200 bp in size. Libraries were amplified by PCR using multiplex oligo following the manufacturer's protocol. Prior to sequencing, libraries were run on an Agilent Bioanalyzer for size and quality control checking. Sequencing was performed in an Illumina HiSeq 2000, generating 50 bp single-ended reads. Input libraries were used as background references for peak identification, sequence alignment, differential expression analysis and identification of H3K9ac-associated peaks.

For ChIPseq analysis, transcripts were aligned to the mm10 reference genome using Bowtie 2-2.2.3, sorting reads in Samtools-0.1.19. Genomic bins of 1,000 bp upstream and downstream of each transcription start site for each gene were created using the same gene annotation as used for the RNAseq data. Read counts per genomic bin were obtained from the mapped reads using HTSeq-0.6.1, and subsequently, differential binding testing was conducted in edgeR-3.8.6. Quality examination on aligned reads was performed using ChIPQC-1.2.2. The cut-off criteria for the differentially occupied genes by H3K9ac were set at $P < 0.05$. ChIP signal distribution plots were generated using NGSplot version 2.47.1. Briefly, the ChIP signal for each condition is plotted along a gene body region either for all genes in the annotation or a select subset of genes. The expression and differential expression data from the RNAseq experiment were used to select the groups of genes to sample the ChIP signal in order to correlate the ChIP signal with changes in the gene's expression between biological conditions. The ChIPseq signal tracks were generated using the macs2 bdgcmp command. The signal pileups of the ChIP and input conditions produced by macs2 callpeaks command

were used as the treatment and control inputs, respectively, for the bdgcmp command. The output bedgraph reports the $-\log_{10}(P \text{ value})$ of treatment relative to control for each bin using the “-m ppois” option. The bedgraph files were then converted to bigwig files using the bedGraphToBigWig utility from KentUtils. The RNAseq signal tracks were created using the deeptools utility, bamCoverage. The bam files of each replicate per condition were pooled together for use as input to bamCoverage (Ramirez *et al*, 2016).

HDAC3 network

The signalling network was generated using the protein interactome (calculated with FpClass, score ≥ 0.8) of HDAC3- and H3K9ac-dependent genes (genes upregulated ($P < 0.05$)) following SNA with an increased H3K9ac occupancy ($P < 0.05$). Only upregulated proteins after SNA were used to build the network. Any nodes in which no connections were found were removed from the output. The network was visualized using Cytoscape software (version 3.3.0), circularizing the terms that have been found enriched for signalling pathways in a KEGG enrichment analysis ($P < 0.05$, see Dataset EV5).

Immunoblotting

Proteins from either sciatic DRGs or dissociated DRG neurons were extracted using RIPA buffer with protease and phosphatase inhibitor cocktails (Roche). Total lysates were obtained by 30' centrifugation at 4°C. Nuclear/cytoplasmic protein lysates from DRGs were extracted using the NE-PER Nuclear and Cytoplasmic Extraction Reagents (Thermo Scientific) following the manufacturer's instruction. Protein concentration of lysate was quantified using Pierce BCA Protein Assay Kit (Thermo Scientific). 10–50 µg of proteins were loaded to SDS-PAGE gels and transferred with iBlot Dry Blotting System (Thermo Scientific). Membranes were blocked with 5% BSA or milk for 1 h RT and incubated with HDAC3 (1:1,000, Abcam), pHDAC3 (1:1,000, Cell Signaling Technology (CST)), H3K9ac (1:1,000, CST), H3 (1:1,000, CST), H3 (1:1,000, CST), GAPDH (1:1,000, CST), ERK (1:1,000, CST), pERK (1:1,000, CST) or PP2A (1:500, Santa Cruz) at 4°C O/N. Following HRP-linked secondary antibody (GE Healthcare) incubation for 1 h RT, membranes were developed with ECL substrate (Thermo Scientific).

Immunocytochemistry

Glass coverslips were coated with 0.1 mg/ml PDL, washed and coated with mouse laminin 2 µg/ml (Millipore). For myelin experiments, they were additionally coated with 4 µg/cm² rat myelin. Cells were plated on coated coverslips for 12 h, at which time they were fixed with 4% paraformaldehyde/4% sucrose. Immunocytochemistry was performed by incubating fixed cells with anti-βIII tubulin (Tuj1, 1:1,000, Promega), GFP: (1:1,000, Abcam), HDAC3 (1:1,000, Abcam), pHDAC3 (1:200, CST), H3K9ac (1:1,000, CST), PP4c (1:200, Santa Cruz) or anti-V5 (1:200, Millipore) antibodies at 4°C O/N. This was followed by incubation with Alexa Fluor 564- or 488-conjugated goat secondary antibodies according to standard protocol (Invitrogen). All cells were counterstained with Hoechst (Molecular Probes).

Immunohistochemistry (IHC)

Dissected DRG were fixed in 4% PFA and transferred to 30% sucrose at 4°C overnight. Tissues were embedded in OCT compound (Tissue-Tek), frozen and cryosectioned. 10-µm tissue sections were permeabilized and blocked in 10% NGS, 0.3% Triton X-100, PBST for 1 h at RT followed by primary antibodies incubation with βIII tubulin (Tuj1, 1:1,000, Promega), GFP: (1:1,000, Abcam), HDAC3 (1:1,000, Abcam), pHDAC3 (1:200, CST), H3K9ac (1:1,000, CST), anti-V5 (1:200, Millipore), p-Stat3 (1:100, CST, #9145), c-Jun (1:50, CST, #9165), ATF3 (1:100, Santa Cruz, sc-188), pErk (1:250, CST, #9101), IGF1R (1:200, CST, #3027), Myc (1:100, Sigma, M4439) and NF200 (Rabbit, 1:80, Sigma, N4142; mouse, 1:400, Sigma, N0142) at 4°C O/N. This was followed by incubation with Alexa Fluor 564- or 488-conjugated goat secondary antibodies according to standard protocol (Invitrogen). All sections were counterstained with Hoechst (Molecular Probes).

Image analysis for IHC and ICC

Dorsal root ganglia or spinal cord was taken at 20× magnification with an Axioplan 2 (Zeiss) microscope and processed with the software AxioVision (Zeiss). Exposure time and gain were maintained constant between conditions for each fluorescence channel. A modified protocol based on the guidelines described on Protocol Exchange (2012) (<https://doi.org/10.1038/protex.2012.008>) was used to quantify fluorescence intensity. Briefly, using ImageJ, a constant fluorescence intensity threshold was set across samples. Based on the threshold, for each picture the intensity density (ID) of pixels was calculated in each channel and then divided by its respective number of cells (about 225 cells/picture). DAPI counterstaining was used to label nuclei. This was done in triplicate and blind to the experimental group.

Neurite length analysis

Immunofluorescence was detected using an Axiovert 200 microscope (Zeiss), and pictures were taken as a mosaic at 10× magnification using a CDD camera (AxioCam MRm, Zeiss). Five fields per coverslip were included in the analysis. All analyses were performed in blind. Neurite analysis and measurements were performed using Neurite-J plugin for ImageJ software (ImageJ). Approximately between 30 and 50 cells were analysed per each condition. Total neurite length per neuron was quantified and averaged.

HDAC3 activity

HDAC3 activity was measured by measuring HDAC activity on DRGs after central and peripheral injury prior to HDAC3 immunoprecipitation. Briefly, sciatic DRGs from 3 animals were extracted 24 h after surgery and pooled per sample, protein lysates were obtained using non-denaturizing lysis buffer (NDLB, 20 mM Tris-HCl pH 8, 137 mM NaCl, 1% IGEPAL, 2 mM EDTA), and for the HDAC3 immunoprecipitation, total lysates were bound to HDAC3 antibody (rabbit, Abcam), pulled down with Protein G Magnetic Beads, washed with NDLB, eluted with 0.1 M glycine pH 2 and neutralized with Tris pH 8. Activity of samples of 20 µg of immunoprecipitated HDAC3 was measured with fluorometric histone

deacetylase activity kit (Active Motif, Rixensart, Belgium) according to the manufacturer’s guidelines.

Intrathecal catheter and osmotic minipump implantation

For RGFP966 delivery, osmotic minipumps (Alzet 2002) were used. A customized 32G i.t. catheter (ReCathCo) was placed subdurally from T11 to T9 caudally connecting osmotic minipump with vehicle or RGFP966 placed in subcutaneous space on the back of mouse. The whole instrument was fixed with cyanoacrylate (Cyano Veneer, Hager & Werken) on muscle-cleaned T12 bone. All pumps were removed at 14 days after injury. Immediately after pump implantation, a T9-T10 laminectomy was performed and a dorsal overhemi-section was performed with a microblade (Fine Science Tools).

In vivo AAV-V5/mutant HDAC3 injection

Briefly, mice were anaesthetized with isoflurane inhalation and sciatic nerves were exposed bilaterally. 1.5–2 µl of AAV1-virus were injected with glass-pulled capillary. A dorsal column crush (30 s) injuring mainly ascending sensory tracts from dorsal columns was performed with a fine #5 microsurgery forceps (Fine Science Tools) 2 weeks after viral injection.

Tracing and tissue processing of injured spinal cords

Five weeks after SCI, 2 µl of tracer (15% Dextran, Alexa Fluor 555, 10000 MW, Thermo Scientific) was injected into sciatic nerve bilaterally. Spinal cords were dissected 5 days after tracing following transcardial perfusion with PBS and 4% PFA, and subsequently cryopreserved with 30% sucrose overnight at 4°C. Spinal cords were mounted and frozen in OCT mounting media and sectioned at 18 µm on a cryostat. Subsequent GFAP (1:500, Millipore), CD11b (1:1,000, Millipore) or VGLUT1 (1:500, Synaptic Systems) stainings were performed as previously described. The GFAP⁺ scar and the CD11b⁺ immunoreactivity within the GFAP-positive area were quantified by calculating pixel intensity. A high-resolution image was obtained at 40× magnification using the Zeiss Axioplan Microscope (Axiovert 200, Zeiss Inc.). Images for the same antigen groups were processed with the same exposure time. Assessment of fluorescence intensity was performed using AlphaEase FC 4.0.1 software by measuring the intensities specifically within the borders of GFAP⁺ scar. At least three sections per sample were quantified. The intensity values of each cell were normalized to the background fluorescent signal, and mean values of intensities were calculated for each animal.

Transfection efficiency of viruses and plasmids

	<i>In vitro/In vivo</i>	Efficiency	Related data
Viruses			
AAV-GFP	<i>In vitro</i>	83.28% ± 6.93	Fig 1-F; Supp Fig 1-C
AAV-HDAC3	<i>In vitro</i>	87.69% ± 5.23	Fig 1-F
AAV-HDAC3mut	<i>In vitro</i>	86.65% ± 5.79	Fig 1-F; Supp Fig 1-C

* (continued)

	<i>In vitro/In vivo</i>	Efficiency	Related data
AAV-V5	<i>In vivo</i>	72.51% ± 8.19	Fig 7-A, C, D; Supp Fig 8-A
AAV-HDAC3mut	<i>In vivo</i>	71.46% ± 7.92	Fig 7-B, E, F; Supp Fig 8-A, B
Plasmids/siRNA			
GFP/scr siRNA	<i>In vitro</i>	36.57% ± 3.34	Fig 4-A
GFP/PP4c siRNA	<i>In vitro</i>	32.22% ± 1.92	Fig 4-B

Quantification of axonal regeneration

For each spinal cord after dorsal column injury, the number of fibres rostral to the lesion and their distance from the lesion epicentre were analysed in 4–6 sections per animal with a fluorescence Axioplan 2 (Zeiss) microscope and with the software Stereo-Investigator 7 (MBF Bioscience). The lesion epicentre (GFAP) was identified in each section at 40× magnification. The total number of labelled axons rostral to the lesion site was normalized to the total number of labelled axons caudal to the lesion site counted in all the analysed sections for each animal, obtaining an inter-animal comparable ratio. Sprouts and regrowing fibres were defined following the anatomical criteria reported by Steward and colleagues (Steward *et al.*, 2003).

HDAC3 RNA silencing

For HDAC3 RNA silencing, shRNA against mouse HDAC3 and scramble shRNA were designed using BLOCK-IT RNAi Designer tool (Life Technologies) and cloned into pRNAT-U6.1/Neo (GenScript) that carries GFP marker, allowing tracking of the transfected cells. The sequences of the shRNAs were as follows: sense: GGATCCC (GGGTGCTCTACATTGATATCG)TTGATATCCG(CGATATCAATGTA GAGCACCC)TTTTTCCAAAAGCTT; anti-sense: GGATCCC(GCCGC TACTATTGTCTCAATG)TTGATATCCG(CATTGAGACAATAGTAGCG GC)TTTTTCCAAAAGCTT; sense: GGATCCC(GACAGGTCTCTGGA ACGTTAT)TTGATATCCG(ATAACGTTCCAGAGACCTGTC)TTTTTT CAAAAGCTT; anti-sense: GGATCCC(ATAGTTGTACTCGGTAC GGT)TTGATATCCG(ACCGTACGCGAGTACAACCTAT)TTTTTCCAA AAGCTT, where the sense and anti-sense strand, separated by a loop, indicated between brackets. Briefly, 25,000–30,000 DRG/ transfection were washed three times after dissociation with PBS w/ o Ca²⁺/Mg²⁺ and transfected using the Neon Transfection System (Life Technologies). Cells were resuspended in 11 microlitres of buffer R and transfected with 1 microgram of DNA at 1,200 mV, 2 pulses, 20 ms. After recovery, cells were plated in medium w/o antibiotics and after 48 h in culture were fixed and analysed.

H3K9ac CHIP-PCR

Lumbar L1–L6 DRGs were extracted as described above, 24 h after dorsal column axotomy surgeries plus intrathecal injection of 5 µl of RGFP966 or vehicle (5% DMSO in 0.9% saline). Tissues from five animals were pooled per sample. Briefly, DRG pellets were crushed using a pestle and chemically cross-linked with a 1%

formaldehyde solution containing 50 mM Hepes-KOH pH7.5, 100 mM NaCl, 1 mM EDTA and 0.5 mM EDTA, for 15 min at room temperature. Nuclear extracts were then sonicated for 10 min by using a tip sonicator, and successful chromatin shearing (200–800 bp) was confirmed by agarose gel analysis. Immunoprecipitation was performed overnight with Protein G Dynabeads (Invitrogen) bound to 5 µg of H3K9ac (Abcam 10812) or Rabbit IgG. After washing, elution and reverse cross-linking, DNA was treated with RNase A and Proteinase K and purified using Qiagen PCR purification columns. Real-time qPCR was run LightCycler 480 SYBR Green I Master (Roche) in a StepOnePlus Cyclor (Applied Biosciences). C_ts were calculated following the manufacturer's instructions. Expression values are expressed as 2^{-ΔΔC_t}. First, ChIP C_ts were normalized versus IgG to exclude non-specificity (ΔC_t); then, the amount of chromatin was normalized using ΔC_t from the input. Primers were designed based on H3K9ac enrichment after H3K9ac ChIPseq. Primer sequences used were as follows:

	Forward (5'-3')	Reverse (5'-3')
Jak1	GGCCATAAACAGGATGTCG	CACGGAAGTGGTGAGTGCC
SOCS3	TTCCTACCTAGTCCCGAAGC	GCCCCTTGTAGACTTCACG
STAT3	CACTCTCTCTCCGCATCTCC	GGTGCTTAGAGCTGTGAATGG
ATF3	GAGGGAACTTAGGGTGAGG	CAGCCACAGTCTCACTCAGC
Jun	CTCTGGGTGAGGAAAGTTGC	GTATTTGGGGAGCATTGG
Fos	CTCTCCTGTCAACACACAGG	TCAGACAAGTCTGGGTTCC
IGF1R	CGCTATTCATTTCCACTCC	AAGAGGAGCAAAGCCCAAT
RhoA	TGATCGGCAAGCACTTTTCC	AGAGGAAGCGACGAGGAGG

Analysis of the HDAC3 interactome

To identify how HDAC3 may interact and function at the protein level, an *in silico* analysis was performed using FpClass prediction software to predict high-confidence protein–protein interactions. Interactions were considered significant when the total score was ≥ 0.4.

Transcription factor binding site analysis

In order to identify common regulators of the genes that were upregulated in association with increased H3K9ac occupancy, transcription factor binding site enrichment analysis was performed using Pscan software (Zambelli *et al.*, 2009). Predicted transcription factor binding motifs were screened within the JASPAR 2016 database, and enrichment of overrepresented consensus sequences in the promoter region of input genes (–450 bp to +50 bp) was computed against the *mus musculus* background dataset. Motifs were considered significant when Bonferroni *P* < 0.05. Predicted TFs that could bind to HDAC3 were identified through integration with FpClass HDAC3 predicted PPI (total score ≥ 0.4).

Gene Ontology and pathway analysis

Gene Ontology (GO) and KEGG pathway analysis were performed in DAVID (<https://david.ncicrf.gov/>). Enrichment terms were considered significant when *P* < 0.05.

Quantitative real-time PCR

Total RNA from bilateral sciatic DRG was extracted 24 h after peripheral or central injuries as described above by using RNeasy Kit (Qiagen) according to the manufacturer’s guidelines. cDNA was then synthesized with SuperScript™ II Reverse Transcriptase (Invitrogen). Real-time qPCR was run with KAPA SYBR FAST qPCR Kit (Kapa Biosystems) in a 7500 LightCycler (Applied Biosciences). C_s were calculated following the manufacturer’s instructions. Expression values are expressed as 2^{-ΔΔC_t}. First, C_s were normalized versus GAPDH as a housekeeping gene, and t, the relative amount, was normalized against corresponding sham controls. Primer sequences used were as follows:

	Forward (5'-3')	Reverse (5'-3')
GAPDH	ACCTGTGCTGTAGCCGTATCA	TCAACAGCAACTCCCCTCTCCA
HDAC1	GAATCCGCATGACTCACAAATT	TCAACAAGCCATCAAACACC
HDAC2	AACCGGCAACAACTGATATG	TTCCAGGAAAGTATTCCCCAT
HDAC3	CCTTTCCAGCCAGTCATCAG	AACATTCGGACAGTGATGCC

Statistical analysis

Unless otherwise stated, data are plotted as the mean ± s.e.m. All experiments were performed three times unless specified. Normality of the distributions was checked via Shapiro–Wilk test, and asterisks indicate a significant difference analysed by ANOVA with Bonferroni post hoc test or Student’s t-test as indicated (*P < 0.05; **P < 0.01; ***P < 0.005; ****P < 0.001). All tests performed were two-sided, and adjustments for multiple comparisons and/or significantly different variances (Fisher’s F) were applied where indicated. All data analysis performed was blinded to the experimental group.

Unless otherwise stated, sample size was chosen in order to ensure a power of at least 0.8, with a type I error threshold of 0.05, in view of the minimum effect size that was expected.

Data availability

RNAseq and H3K9ac ChIPseq data have been deposited at the Gene Expression Omnibus (GEO) with accession codes: GSE97090 for RNAseq, <https://www.ncbi.nlm.nih.gov/geo/query/acc.cgi?acc=GSE97090> and GSE108806 (<https://www.ncbi.nlm.nih.gov/geo/query/acc.cgi?acc=GSE108806>) for ChIPseq.

Expanded View for this article is available online.

Acknowledgements

We would like to thank start-up funds—Division of Brain Sciences, Imperial College London (SDG), the Hertie Foundation for financial support (SDG); Wings for Life (SDG); the DFG (SDG); the Henry Smith Charity; and Rosetrees Trust (SDG). The research was supported by the National Institute for Health Research (NIHR) Imperial Biomedical Research Centre (SDG) and the Spanish Ministry of Economy, Industry and Competitiveness (MEICO; BFU2015-67777-R, JADR; IJCI-2016-30783, AH). The views expressed are those of the author(s)

and not necessarily those of the NHS, the NIHR or the Department of Health.

Author contributions

AH performed and designed experiments, performed data analysis and wrote the manuscript; LZ performed and designed experiments and performed data analysis; IP performed and designed experiments and performed data analysis; EM performed experiments and data analysis, GK performed experiments; TH performed experiments; MCD performed data analysis; VPL supervised experiments and edited the manuscript; JLB contributed to manuscript writing; AM-A performed experiments; KF performed and designed experiments; FDV performed and designed experiments and data analysis; DPM produced and provided expertise on materials used in the manuscript; JK produced and provided expertise on materials used in the manuscript; MAW produced and provided expertise on materials used in the manuscript and performed experiments; RP designed experiments and provided technical support; JAR supported and supervised experiments and edited the manuscript; SDG designed experiments, performed data analysis and wrote the manuscript.

Conflict of interest

The authors declare that they have no conflict of interest.

References

Barlow DP (1992) Preparation, restriction, and hybridization analysis of Mammalian genomic DNA for pulsed-field gel electrophoresis. *Methods Mol Biol* 12: 107–128

Bose P, Dai Y, Grant S (2014) Histone deacetylase inhibitor (HDACI) mechanisms of action: emerging insights. *Pharmacol Ther* 143: 323–336

Cho Y, Sloutsky R, Naegle KM, Cavalli V (2013) Injury-induced HDAC5 nuclear export is essential for axon regeneration. *Cell* 155: 894–908

Chong MS, Reynolds ML, Irwin N, Coggeshall RE, Emson PC, Benowitz LI, Woolf CJ (1994) GAP-43 expression in primary sensory neurons following central axotomy. *J Neurosci* 14: 4375–4384

Di Giovanni S, Knights CD, Rao M, Yakovlev A, Beers J, Catania J, Avantiaggiati ML, Faden AI (2006) The tumor suppressor protein p53 is required for neurite outgrowth and axon regeneration. *EMBO J* 25: 4084–4096

Finelli MJ, Wong JK, Zou H (2013) Epigenetic regulation of sensory axon regeneration after spinal cord injury. *J Neurosci* 33: 19664–19676

Floriddia EM, Rathore KI, Tedeschi A, Quadrato G, Wuttke A, Lueckmann JM, Kigerl KA, Popovich PG, Di Giovanni S (2012) p53 regulates the neuronal intrinsic and extrinsic responses affecting the recovery of motor function following spinal cord injury. *J Neurosci* 32: 13956–13970

Gaub P, Tedeschi A, Puttagunta R, Nguyen T, Schmandke A, Di Giovanni S (2010) HDAC inhibition promotes neuronal outgrowth and counteracts growth cone collapse through CBP/p300 and P/CAF-dependent p53 acetylation. *Cell Death Differ* 17: 1392–1408

Gaub P, Joshi Y, Wuttke A, Naumann U, Schnichels S, Heiduschka P, Di Giovanni S (2011) The histone acetyltransferase p300 promotes intrinsic axonal regeneration. *Brain* 134: 2134–2148

He X, Zhang L, Queme LF, Liu X, Lu A, Waclaw RR, Dong X, Zhou W, Kidd G, Yoon SO et al (2018) A histone deacetylase 3-dependent pathway delimits peripheral myelin growth and functional regeneration. *Nat Med* 24: 338–351

Hervera A, De Virgiliis F, Palmisano I, Zhou L, Tantardini E, Kong G, Hutson T, Danzi MC, Perry RB, Santos CXC et al (2018) Reactive oxygen species

- regulate axonal regeneration through the release of exosomal NADPH oxidase 2 complexes into injured axons. *Nat Cell Biol* 20: 307–319
- Karagianni P, Wong J (2007) HDAC3: taking the SMRT-N-CoRrect road to repression. *Oncogene* 26: 5439–5449
- Kim CF, Moalem-Taylor G (2011) Detailed characterization of neuro-immune responses following neuropathic injury in mice. *Brain Res* 1405: 95–108
- Kim D, You B, Lim H, Lee SJ (2011) Toll-like receptor 2 contributes to chemokine gene expression and macrophage infiltration in the dorsal root ganglia after peripheral nerve injury. *Mol Pain* 7: 74
- Kretsovali A, Hadjimichael C, Charmpilas N (2012) Histone deacetylase inhibitors in cell pluripotency, differentiation, and reprogramming. *Stem Cells Int* 2012: 184154
- Kuboyama T, Wahane S, Huang Y, Zhou X, Wong JK, Koemeter-Cox A, Martini M, Friedel RH, Zou H (2017) HDAC3 inhibition ameliorates spinal cord injury by immunomodulation. *Sci Rep* 7: 8641
- Kwapis JL, Alaghand Y, Lopez AJ, White AO, Campbell RR, Dang RT, Rhee D, Tran AV, Carl AE, Matheos DP et al (2017) Context and auditory fear are differentially regulated by HDAC3 activity in the lateral and basal Subnuclei of the Amygdala. *Neuropsychopharmacology* 42: 1284–1294
- Lahm A, Paolini C, Pallaoro M, Nardi MC, Jones P, Neddermann P, Sambucini S, Bottomley MJ, Lo Surdo P, Carfi A et al (2007) Unraveling the hidden catalytic activity of vertebrate class IIa histone deacetylases. *Proc Natl Acad Sci USA* 104: 17335–17340
- Lindner R, Puttagunta R, Nguyen T, Di Giovanni S (2014) DNA methylation temporal profiling following peripheral versus central nervous system axotomy. *Sci Data* 1: 140038
- Mason MR, Lieberman AR, Grenningloh G, Anderson PN (2002) Transcriptional upregulation of SCG10 and CAP-23 is correlated with regeneration of the axons of peripheral and central neurons *in vivo*. *Mol Cell Neurosci* 20: 595–615
- McGraw J, Oschipok LW, Liu J, Hiebert GW, Mak CF, Horie H, Kadoya T, Steeves JD, Ramer MS, Tetzlaff W (2004) Galectin-1 expression correlates with the regenerative potential of rubrospinal and spinal motoneurons. *Neuroscience* 128: 713–719
- Neumann S, Woolf CJ (1999) Regeneration of dorsal column fibers into and beyond the lesion site following adult spinal cord injury. *Neuron* 23: 83–91
- Neumann S, Bradke F, Tessier-Lavigne M, Basbaum AI (2002) Regeneration of sensory axons within the injured spinal cord induced by intraganglionic cAMP elevation. *Neuron* 34: 885–893
- Puttagunta R, Schmandke A, Floriddia E, Gaub P, Fomin N, Ghyselinck NB, Di Giovanni S (2011) RA-RAR- β counteracts myelin-dependent inhibition of neurite outgrowth via Lingo-1 repression. *J Cell Biol* 193: 1147–1156
- Puttagunta R, Tedeschi A, Soria MC, Hervera A, Lindner R, Rathore KI, Gaub P, Joshi Y, Nguyen T, Schmandke A et al (2014) PCAF-dependent epigenetic changes promote axonal regeneration in the central nervous system. *Nat Commun* 5: 3527
- Ramirez F, Ryan DP, Gruning B, Bhardwaj V, Kilpert F, Richter AS, Heyne S, Dundar F, Manke T (2016) deepTools2: a next generation web server for deep-sequencing data analysis. *Nucleic Acids Res* 44: W160–W165
- Stam FJ, MacGillavry HD, Armstrong NJ, de Gunst MC, Zhang Y, van Kesteren RE, Smit AB, Verhaagen J (2007) Identification of candidate transcriptional modulators involved in successful regeneration after nerve injury. *Eur J Neurosci* 25: 3629–3637
- Steward O, Zheng B, Tessier-Lavigne M (2003) False resurrections: distinguishing regenerated from spared axons in the injured central nervous system. *J Comp Neurol* 459: 1–8
- Tedeschi A, Nguyen T, Puttagunta R, Gaub P, Di Giovanni S (2009) A p53-CBP/p300 transcription module is required for GAP-43 expression, axon outgrowth, and regeneration. *Cell Death Differ* 16: 543–554
- Teng FY, Tang BL (2006) Axonal regeneration in adult CNS neurons—signaling molecules and pathways. *J Neurochem* 96: 1501–1508
- Togi S, Kamitani S, Kawakami S, Ikeda O, Muromoto R, Nanbo A, Matsuda T (2009) HDAC3 influences phosphorylation of STAT3 at serine 727 by interacting with PP2A. *Biochem Biophys Res Comm* 379: 616–620
- Tonra JR, Curtis R, Wong V, Cliffer KD, Park JS, Timmes A, Nguyen T, Lindsay RM, Acheson A, DiStefano PS (1998) Axotomy upregulates the anterograde transport and expression of brain-derived neurotrophic factor by sensory neurons. *J Neurosci* 18: 4374–4383
- Winfree LM, Speese SD, Logan MA (2017) Protein phosphatase 4 coordinates glial membrane recruitment and phagocytic clearance of degenerating axons in *Drosophila*. *Cell Death Dis* 8: e2623
- Zambelli F, Pesole G, Pavesi G (2009) Pscan: finding over-represented transcription factor binding site motifs in sequences from co-regulated or co-expressed genes. *Nucleic Acids Res* 37: W247–W252
- Zhang Y, Roslan R, Lang D, Schachner M, Lieberman AR, Anderson PN (2000) Expression of CHL1 and L1 by neurons and glia following sciatic nerve and dorsal root injury. *Mol Cell Neurosci* 16: 71–86
- Zhang X, Ozawa Y, Lee H, Wen YD, Tan TH, Wadzinski BE, Seto E (2005) Histone deacetylase 3 (HDAC3) activity is regulated by interaction with protein serine/threonine phosphatase 4. *Genes Dev* 19: 827–839